Introduction to Fracture Mechanics

C.H. Wang

Airframes and Engines Division
Aeronautical and Maritime Research Laboratory

DSTO-GD-0103

ABSTRACT

This text is based on a series of lectures conducted on fracture mechanics. As an introductory course, the test is focused on the essential concepts and analytical methods of fracture mechanics, aiming at painting a broad picture of the theoretical background to fracture mechanics. While a brief review of some important issues in the theory of elasticity is provided in the first chapter, the main focus of the test is centred on stress analysis and energetic approaches to cracked components, local plastic deformation at crack tips, fracture criteria and fatigue life prediction.

DEPARTMENT OF DEFENCE

DEFENCE SCIENCE AND TECHNOLOGY ORGANISATION

Published by

DSTO Aeronautical and Maritime Research Laboratory
PO Box 4331
Melbourne Victoria 3001

Telephone: (03) 9626 8111
Fax: (03) 9626 8999

AR No. AR-009-786
July 1996

APPROVED FOR PUBLIC RELEASE

Introduction to Fracture Mechanics

Executive Summary

This text is prepared for a series of lectures on fracture mechanics. The main aim of the lectures is to provide AMRL staff who are involved in aircraft fatigue and fracture research with a broad picture of the theoretical background to fracture mechanics via a stress analysis viewpoint.

As an introductory course, the lectures are focused on the essential concepts and analytical methods of fracture mechanics. A brief review of some important issues in the theory of elasticity is provided in Chapter 1, while the remaining chapters deal with the stress analysis approach and the energy approach to cracked components, local plastic deformation at crack tips, fracture criteria and fatigue life prediction.

Authors

C. H. Wang

Airframe and Engine Division

Chun-Hui Wang has a B.Eng and Ph.D (Sheffield, UK) in Mechanical Engineering and is currently a member of the Institute of Engineers, Australia. Prior to joining the Aeronautical and Maritime Research Laboratory in 1995 as a Senior Research Scientist, Dr. Wang was a Lecturer at the Deakin University. He has an extensive research record in fatigue and fracture mechanics, stress analysis and constitutive modelling, and biomechanics. Over the last six years he also held academic/research positions at the University of Sydney and the University of Sheffield, UK.

Contents

1. Fundamentals

1.1 Historical Overview

All engineering components and structures contain geometrical discontinuities - threaded connections, windows in aircraft fuselages, keyways in shafts, teeth of gear wheels, etc. The size and shape of these features are important since they determine the strength of the artefact. Conventionally, the strength of components or structures containing defects is assessed by evaluating the stress concentration caused by the discontinuity features. However, such a conventional approach would give erroneous answers if the geometrical discontinuity features have very sharp radii. To illustrate this point, consider the following four cases:

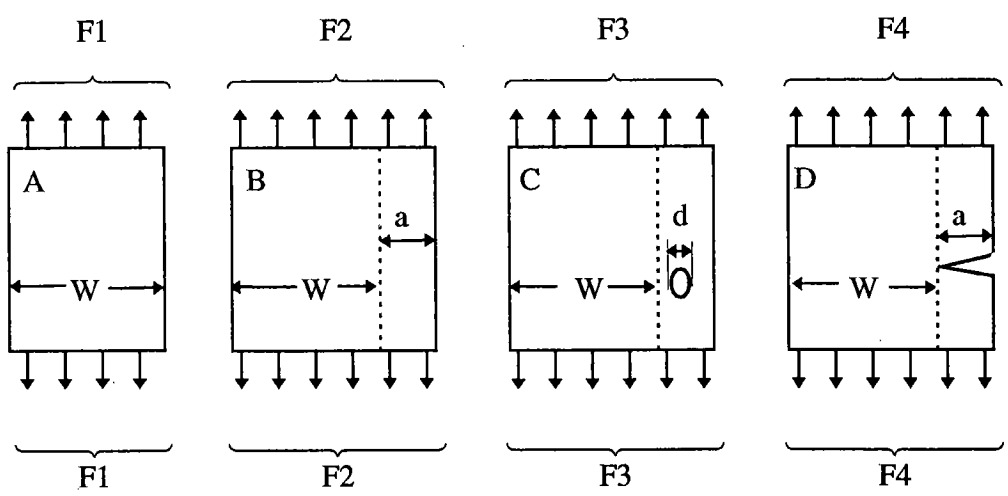

Fig.1.1 Strength of uncracked and cracked plates

The thickness of each plate is the same. The forces required to break the four samples can be arranged in the following order:

$$F4 < F3 < F1 < F2$$

Clearly the sizes of the defects at F_3 and F_4 are crucial to the strength of the structure.

Fracture mechanics is a set of theories describing the behaviour of solids or structures with geometrical discontinuity at the scale of the structure. The discontinuity features may be in the form of line discontinuities in two-dimensional media (such as plates, and shells) and surface discontinuities in three-dimensional media. Fracture mechanics

has now evolved into a mature discipline of science and engineering and has dramatically changed our understanding of the behaviour of engineering materials. One of the important impacts of fracture mechanics is the establishment of a new design philosophy: damage tolerance design methodology, which has now become the industry standard in aircraft design.

'Fracture mechanics' is the name coined for the study which combines the mechanics of cracked bodies and mechanical properties. As indicated by its name, fracture mechanics deals with fracture phenomena and events. The establishment of fracture mechanics is closely related to some well known diasters in recent history. Several hundred liberty ships fractured extensively during World War II. The failures occurred primarily because of the change from riveted to welded construction and the major factor was the combination of poor weld properties with stress concentrations, and poor choice of brittle materials in the construction. Of the roughly 2700 liberty ships built during World War II, approximately 400 sustained serious fracture, and some broke completely in two. The Comet accidents in 1954 sparked an extensive investigation of the causes, leading to significant progress in the understanding of fracture and fatigue. In July 1962 the Kings Bridge, Melbourne failed as a loaded vehicle of 45 tonnes crossing one of the spans caused it to collapse suddenly. Four girders collapsed and the fracture extended completely through the lower flange of the girder, up the web and in some cases through the upper flange. Remarkably no one was hurt in the accident.

Fracture mechanics can be divided into linear elastic fracture mechanics (LEFM) and elasto-plastic fracture mechanics (EPFM). LEFM gives excellent results for brittle-elastic materials like high-strength steel, glass, ice, concrete, and so on. However, for ductile materials like low-carbon steel, stainless steel, certain aluminium alloys and polymers, plasticity will always precede fracture. Nonetheless, when the load is low enough, linear fracture mechanics continues to provide a good approximation to the physical reality. The purpose of this lecture is to provide a broad picture of the theoretical background to fracture mechanics via a stress analysis view point.

1.2 Notches and Stress Concentration

There seems to be confusion among many engineers between notches and cracks. This is not surprising as the boundary between notch and crack is sometimes blurred, especially under fatigue conditions.

A notch is defined as geometric discontinuity which has a definite depth and root radius. Examples are bolt holes, screw threads or oil holes. The effect of a notch on a tensile stress field is easily visualised by the familiar 'stress flow' analogy which illustrates the high 'density' of stress around the root of a notch, Fig.2. This analogy is very useful in deciding upon an apparently contradictory course of action: removing or adding material to smooth out the flow of stress, hence making component stronger. For instance, if we remove the material (width = a) in Fig.1, we can recover the loss of strength in cases C and D to the same level as in case A.

The stress concentration factor, K_T, which reflects the severity of a notch, is defined as the dimensionless ratio of the maximum (elastic) stress at the root of a notch, to the

nominal applied stress. The suffix T derives historically from theoretical elasticity theory. The stress concentration factor can be evaluated using analytical, numerical and experimental techniques; for common notch shapes the K_T values can also be obtained from a wealth of tables and charts. One practical approximation for many notch shapes is the formula for elliptical notch shapes:

$$K_T = \frac{\sigma_{max}}{\sigma_{nom}} = 1 + 2\sqrt{\frac{D}{\rho}} \qquad (1.1)$$

where D and ρ are the notch depth (or half notch diameter) and the notch root radius, respectively. The K_T value for a circular hole is equal to 3, hence relatively shallow notches can cause local notch root stress to rise above the material's strength even for modest values of nominal applied stress. Therefore the presence of a notch can be crucial to the safety of components made of brittle materials. It should be noted that the local maximum stress at failure for a notched component is not strictly constant but may vary with the notch depth. For ductile materials, notches are less dangerous, since the stress gradient ahead of a concentrating feature is steep thus limiting the spread of plasticity to a small region and avoiding plastic collapse. However, this saving grace for static loading can become, and probably is, the greatest single cause of failures in operating plant subjected to repeated loading. This is because fatigue cracks can be initiated in the plastic zone of a notch and become very sharp stress concentrating features (better known as cracks) in their own right, able to propagate under the lower stress level existing within the bulk of the material.

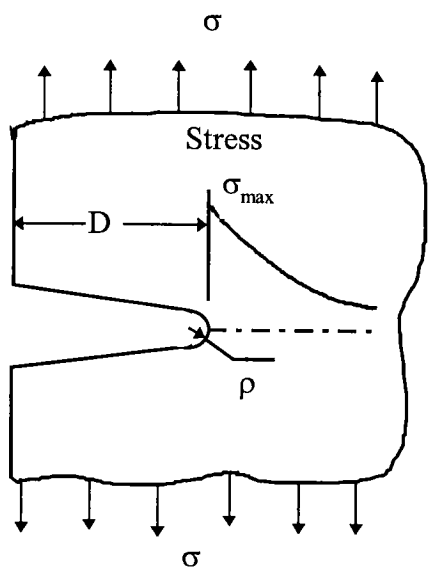

Fig.1.2 Stress concentration

1.3 Cracks and Stress Intensity Factor

From equation (1.1) we can see if we reduce the notch root radius, ρ, to a very small value, even approaching a mathematical zero (in engineering terms, to the order of the dimensions of an atom, 10^{-9}m), the stress concentration factor K_T tends to approach infinity; the geometry is reduced to a crack. As a result, the crack tip stress approaches a theoretical value of infinity, irrespective of notch depth,

$$\sigma_{max} = \lim_{\rho \to 0} S(1+2\sqrt{\frac{D}{\rho}}) \approx 2S \lim_{\rho \to 0} \sqrt{\frac{D}{\rho}} \tag{1.2}$$

Clearly the idea of stress concentration factor breaks down for a crack, since it cannot distinguish between various crack lengths and applied stress levels.

It is interesting, however, to examine a product,

$$\frac{1}{2}\sigma_{max}\sqrt{\pi\rho} = \frac{1}{2}(2S\sqrt{\frac{D}{\rho}})\sqrt{\pi\rho} = S\sqrt{\pi D} \tag{1.3}$$

which remains finite and contains the information of remote applied load and the size of the crack. As we will see later, this new parameter is the so called 'stress intensity factor'.

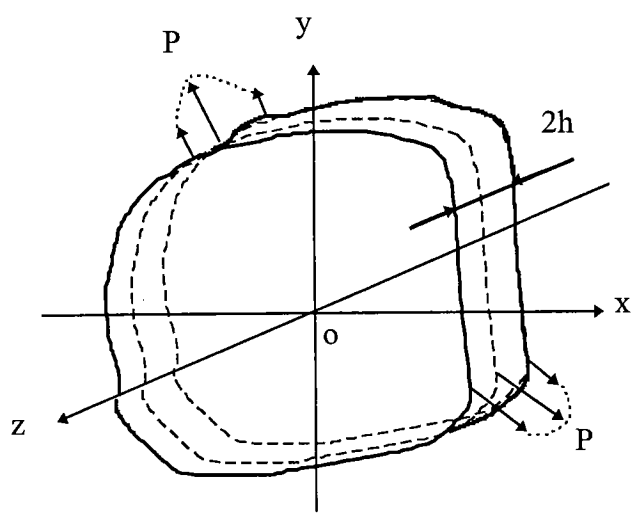

Fig.1.3 Plane stress state

1.4 Plane Stress and Plane Strain

Plane stress: a thin plate loaded with forces parallel to its plane and distributed symmetrically over the whole thickness. Stress components $\sigma_z, \tau_{zx}, \tau_{zy}$ are zero and

there are only three nonzero stress components: $\sigma_x, \sigma_y, \tau_{xy}$. The stress and strain tensors can be written as,

Stress tensor:
$$\begin{vmatrix} \sigma_x & \tau_{xy} & 0 \\ \tau_{xy} & \sigma_y & 0 \\ 0 & 0 & 0 \end{vmatrix}$$

Strain tensor:
$$\begin{vmatrix} \varepsilon_x & \gamma_{xy} & 0 \\ \gamma_{xy} & \varepsilon_y & 0 \\ 0 & 0 & \varepsilon_z \end{vmatrix}$$

where $\varepsilon_z = -\frac{\nu}{E}(\sigma_x + \sigma_y)$

and Hooke's law is

$$\varepsilon_x = \frac{1}{E}(\sigma_x - \nu\sigma_y) \tag{1.4}$$

$$\varepsilon_y = \frac{1}{E}(\sigma_y - \nu\sigma_x) \tag{1.5}$$

$$\gamma_{xy} = \frac{1+\nu}{E}\tau_{xy} \tag{1.6}$$

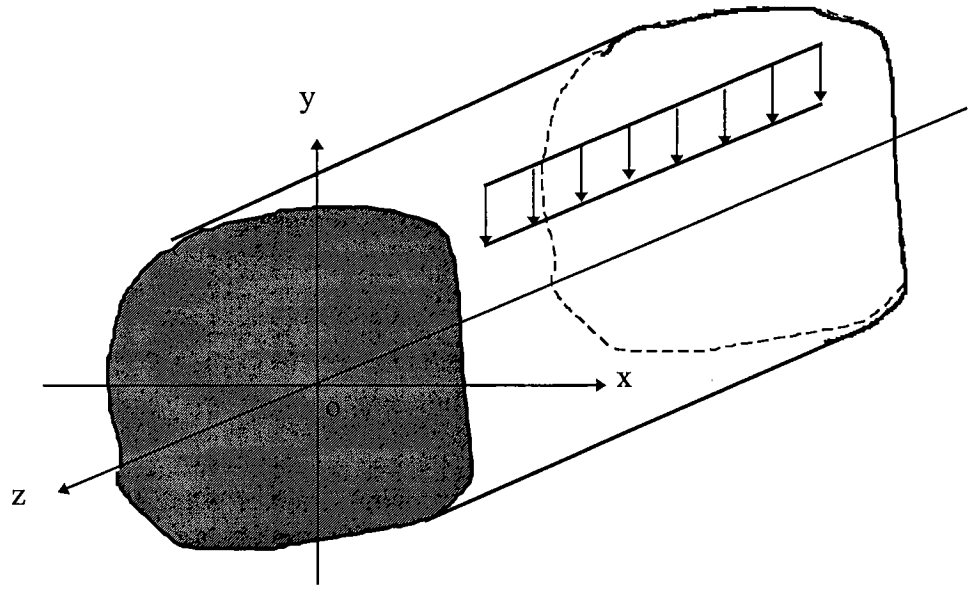

Fig.1.4 Plane strain state

Plane strain: A long cylindrical or prismatical body subjected to forces that are normal to its axis and do not vary along the length. There are three non-zero strain components ($\varepsilon_x, \varepsilon_y, \gamma_{xy}$), as $\varepsilon_z = \gamma_{xz} = \gamma_{yz} = 0$. The stress and strain tensors are,

Stress tensor:
$$\begin{vmatrix} \sigma_x & \tau_{xy} & 0 \\ \tau_{xy} & \sigma_y & 0 \\ 0 & 0 & \sigma_z \end{vmatrix}$$

where $\sigma_z = \nu(\sigma_x + \sigma_y)$

Strain tensor:
$$\begin{vmatrix} \varepsilon_x & \gamma_{xy} & 0 \\ \gamma_{xy} & \varepsilon_y & 0 \\ 0 & 0 & 0 \end{vmatrix}$$

The above Hooke's law for plane stress condition are also applicable if we make the following formal changes to it: substitute constants

$$\nu \text{ by } \nu' = \frac{\nu}{1-\nu} \tag{1.7}$$

$$E \text{ by } E' = \frac{E}{1-\nu^2} \tag{1.8}$$

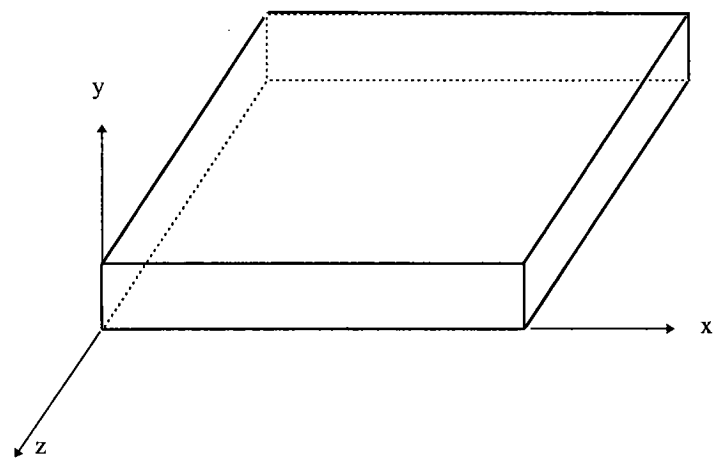

Fig.1.5 Plane stress or plane strain?

There seems to be quite a lot of confusion about plane strain or plane stress. Consider a plate as shown in Fig.1.5: it is a plane stress problem if the plate is subjected to in-plane loading and the interest is about the stresses and deformation in the *xz* plane, otherwise it should be treated as plane strain for both the *xy* and *zy* planes. A rule of thumb is that if the dimension normal to the plane of interest is much greater than the

in-plane dimensions, then it is plane strain, otherwise plane stress. Furthermore, the concept of plane stress or plane strain is mainly for the convenience of 2D representation of actual 3D structure, hence it is relative. In many cases the determining factor is whether there exists a high stress/strain gradient near the point of interest. For example, if the plate shown in Fig.1.5 is subjected to bending in the *xy* or *zy* plane, it should be considered as plane strain state and the effective Young's modulus should be $E/(1-\nu^2)$. This is because the high strain gradient through the plate thickness induced due to Poisson's ratio effect cannot be fully developed.

1.5 Stress Function

From the theory of elasticity it is easy to show that a true solution to a two-dimensional problem must satisfy (i) equilibrium, (ii) compatibility, (iii) boundary conditions. The equations of elasticity reduce to two-dimensional forms in three special cases, as discussed previously:

1. *Plane Strain*: In this case the displacement component u_z is identically equal to zero, and none of the physical quantities depends on *z*.
2. *Plane Stress*: In a state of plane stress parallel to the *xy*-plane, the stress components σ_{xz}, σ_{yz} and σ_{zz} all vanish but the components of the displacement vector are not independent of *z*.
3. *Generalised Plane Stress*: This is a state of stress in a thin plate $-h \le z \le h$ when σ_{zz}=0 throughout the plate but $\sigma_{xz} = \sigma_{yz} = 0$ only on the surfaces $z = \pm h$ of the plate.

For 2D problems, the first two requirements can be automatically satisfied by choosing an Airy stress function, Φ (see Timoshenko,1970) such that,

$$\sigma_x = \frac{\partial^2 \Phi}{\partial y^2} \qquad \sigma_y = \frac{\partial^2 \Phi}{\partial x^2} \qquad \tau_{xy} = -\frac{\partial^2 \Phi}{\partial x \partial y} \tag{1.9}$$

where the stress function is bi-harmonic,

$$\frac{\partial^4 \Phi}{\partial x^4} + 2\frac{\partial^4 \Phi}{\partial x^2 \partial y^2} + \frac{\partial^4 \Phi}{\partial y^4} = 0 \tag{1.10}$$

Thus the solution of a two-dimensional problem, when the weight of the body is only body force, reduces to finding a solution of equation (1.10) that satisfies the boundary conditions of the problem.

A major development in the field of two-dimensional elasticity has been Muskhelishvili's (1953) work on the complex form of the two-dimensional equations. Before we proceed, however, it is necessary to review some fundamental concepts in complex analytic functions. For an analytic function *f*(*z*), where *z*=*x*+*iy*, we have

$$\frac{\partial}{\partial x} f(z) = f'(z) \quad \text{and} \quad \frac{\partial}{\partial y} = if'(z)$$

from which it is easy to show the Cauchy-Riemann conditions[1]. Now let us define

$$\sigma_{xx} + \sigma_{yy} = 2\left[\phi'(z) + \overline{\phi'(z)}\right] = 4\,\mathrm{Re}\,\phi'(z) \tag{1.11a}$$

$$\sigma_{yy} - \sigma_{xx} + 2i\sigma_{xy} = 2\left[\bar{z}\phi''(z) + \chi''(z)\right] \tag{1.11b}$$

$$2(u_x + iu_y) = K\phi(z) - z\overline{\phi'(z)} - \overline{\chi(z)} \tag{1.11c}$$

where K=3-4ν for plane strain and K=(3-ν)/(1+ν) for plane stress. Here the complex variable is z=x+iy, referring to a generic point in the xy plane. Note $\bar{z} = x - iy$. Functions ϕ and χ are arbitrary complex potentials. The transformation of the Muskhelishvili formulas using a comformal mapping method from the z-plane to a ζ-plane (where z=x+iy and $\zeta = \xi + i\gamma$) is of great use in discussing boundary value problems. For further details please see Ref (Muskhelishvili,1953).

Two special cases of the formulas (1.11) are associated with the name of Westergaard (1939). If we make the substitutions,

$$\phi'(z) = \frac{1}{2}Z(z) \qquad \chi'(z) = -\frac{1}{2}zZ'(z) \tag{1.12}$$

where function Z_1 is an analytic function of the complex variable z. It is easy to show that the following function satisfies equation (1.10), noting the Cauchy-Riemann conditions for the differentiation of an analytic complex variable,

$$\Phi = \mathrm{Re}\,\bar{\bar{Z}} + y\,\mathrm{Im}\,\bar{Z} \tag{1.13}$$

where $\bar{Z} = \int Z dz$ and $\bar{\bar{Z}} = \int \bar{Z} dz$. Now equations (1.11) reduce to

$$\sigma_{xx} = \mathrm{Re}\,Z - y\,\mathrm{Im}\,Z' \quad \sigma_{yy} = \mathrm{Re}\,Z + y\,\mathrm{Im}\,Z' \quad \sigma_{xy} = -y\,\mathrm{Re}\,Z' \tag{1.14a}$$

$$2Gu = 2(1-\nu)\,\mathrm{Im}\,\bar{Z} + y\,\mathrm{Re}\,Z \tag{1.15b}$$

$$2Gv = -(1-2\nu)\,\mathrm{Re}\,\bar{Z} - y\,\mathrm{Im}\,Z \tag{1.16c}$$

It should be observed that this solution has the property that, on the line $y = 0$, $\sigma_{xy} = 0$ and $\sigma_{xx} = \sigma_{yy}$. When a conformal mapping is performed, this boundary

---

[1] $\dfrac{\partial \mathrm{Re}\,Z}{\partial x} = \dfrac{\partial \mathrm{Im}\,Z}{\partial y} = \mathrm{Re}\,Z' \qquad \dfrac{\partial \mathrm{Im}\,Z}{\partial x} = -\dfrac{\partial \mathrm{Re}\,Z}{\partial y} = \mathrm{Im}\,Z'$ so $\nabla^2\,\mathrm{Re}\,Z = \nabla^2\,\mathrm{Im}\,Z = 0$

condition represents a plate with a hole subjected to a hydrostatic pressure, for which the stress solution is known.

Similarly, if we make the substitutions

$$\phi'(z) = -\frac{1}{2} iZ_2(z) \qquad \chi'(z) = \frac{1}{2} izZ_2'(z) + iZ_2(z) \tag{1.17}$$

we find the corresponding stress field is given by

$$\sigma_{xx} = 2\,\mathrm{Im}\,Z_2 + y\,\mathrm{Re}\,Z_2' \qquad \sigma_{yy} = -y\,\mathrm{Re}\,Z_2' \qquad \sigma_{xy} = \mathrm{Re}\,Z_2 - y\,\mathrm{Im}\,Z_2' \tag{1.18}$$

This solution has the property that, on the line y=0, $\sigma_{yy} = 0$.

For illustration purposes, let us consider a case of an unstressed elliptic hole in an infinite plate that is subjected to 'all-round' tension. The problem can be solved by using the following simple conformal mapping of the exterior of an ellipse into the interior of a unit circle, for which the stresses are known,

$$z = c\cosh\zeta \tag{1.19}$$

where $z = x + iy$ and $\zeta = \xi + i\gamma$. That is $x = c\cosh\xi\cos\gamma$ and $y = c\sinh\xi\sin\gamma$, representing a curvilinear coordinate system in which the elliptic boundary is defined by $\xi = \alpha$. Detailed solutions for this problem can be found in Ref.(Timoshenko,1970).

2. Stress Analysis of Cracked Components

2.1 Energy Balance During Crack Growth

The obvious difference between a cracked body and an uncracked body is the additional surface associated with a crack. It is a well known fact that creating new (crack) surfaces consumes energies, because surfaces carry higher energy than the body. It then follows that whether or not a stressed cracked body remains stable or becomes unstable is dependent on whether the cracked body contains sufficient energy to afford to creating additional surface while still maintains equilibrium. This is the basic concept that Griffith proposed in the 1920's to formulate a linear elastic theory of crack propagation. To illustrate this point, let us consider an elastic body Γ containing an internal crack of length $2a$, which is subjected to loads applied at the outer boundary S; see Fig.2.1.

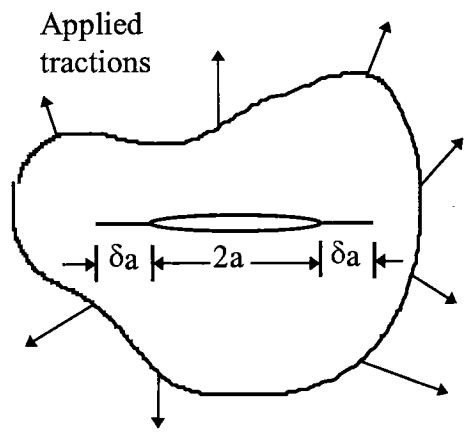

Fig.2.1 Equilibrium and energy balance of a cracked system

According to the law of conservation of energy the work performed per unit time by the applied loads ($\dot{W}$) must be equal to the rates of change of the internal elastic energy ($\dot{U}_E$), plastic energy ($\dot{U}_p$), kinetic energy ($\dot{K}$) of the body, and the energy per unit time ($\dot{\Gamma}$) spent in increasing the crack area. In other words,

$$\dot{W} = \dot{U}_E + \dot{U}_P + \dot{K} + \dot{\Gamma} \qquad (2.1)$$

where a dot over the letter refers to differentiation with respect to time.

If the crack grows slowly the kinematic energy K (or $\dot{K} = 0$) is negligible and can be omitted from the energy balance equation. Since all changes with respect to time are caused by changes in crack size, we have

$$\frac{\partial}{\partial t} = \frac{\partial}{\partial A}\frac{\partial A}{\partial t} = \dot{A}\frac{\partial}{\partial A} \tag{2. 2}$$

where A represents the crack area, and is equal to $2aB$ for the system shown in Fig.2.1. Here B is the thickness of the plate containing the crack and $\dot{A}$ denotes the crack surface area growth rate per unit time. Note that the total crack surface area is twice the area of one crack surface. Therefore equation (2.1) can be rewritten as

$$-\frac{\partial \Pi}{\partial A} = \frac{\partial U_P}{\partial A} + \frac{\partial \Gamma}{\partial A} \tag{2. 3}$$

where

$$\Pi = U_E - W \tag{2. 4}$$

is the potential energy of the system. Equation (2.3) indicates that the reduction of potential energy is equal to the energy dissipated in plastic work and surface creation.

2.2 Griffith Theory

For an ideally brittle material, the energy dissipated in plastic deformation is negligible and can be ignored, i.e. $U_p = 0$. Since the energy spent in increasing the crack area is independent of the crack size, equation (2.3) can be rewritten as

$$-\frac{\partial \Pi}{\partial A} = \frac{\partial \Gamma}{\partial A} = 2\gamma \tag{2.5}$$

where γ represents the energy required to form unit new material surface area. The factor 2 in the above equation refers to the two new material surfaces formed during crack growth. Simply, the above equilibrium equation means that sufficient potential energy must be available in the system to overcome the surface energy of the material. In general, for an elastic body containing a crack, we can define a crack-extension force, G,

$$G = -\frac{\partial \Pi}{\partial A} \tag{2.6}$$

per unit width of crack front. Note that $A = a \cdot B$ when there is only one crack tip (e.g. edge cracked component) and $A = 2a \cdot B$ for centre cracked system. It is important to note the distinction between crack area and surface area. Since a crack includes two matching surfaces, the crack surface area is twice that of the projected crack area, and is equal to $2aB$ in the present case.

We can also define the total energy of the system, which contains three parts: (1) the amount of work done by the applied loads, (2) the elastic energy, and (3) the energy required to form the crack surface. The total energy is

$$U_{total} = (-W + U_E) + \Gamma \tag{2.7}$$

According to *linear* elasticity theory, a body under *constant applied loads* obeys

$$W = 2U_E \tag{2.8}$$

which is sometimes called Clapeyron's theorem of linear elastostatics; a simple proof of which will be shown later. In this case equation (2.6) can be expressed as

$$G = \frac{\partial U_E}{\partial A} \tag{2.9}$$

The total energy of the system is

$$U_{total} = -U_E + \Gamma \tag{2.10}$$

Griffith used the stress solutions by Inglis (1939) to show that the increase in strain energy due to the elliptic cavity (zero radius) in an infinite plane is given by

$$U_E = \frac{\pi a^2 \sigma^2 B}{E} \tag{2.11}$$

where B is the plate thickness, and

$$\Gamma = 4a \cdot B \cdot \gamma \tag{2.12}$$

where γ is the free surface energy per unit area, which is clearly a material constant. Thus, the total system energy becomes, for the case of a thin plate,

$$U_{total} = -\frac{\pi a^2 \sigma^2 B}{E} + 4aB\gamma \tag{2.13}$$

A schematic drawing of the above equation is shown in Fig 2.2, which exhibits a maximum at the following crack length,

$$a_c = \frac{2\gamma E}{\pi \sigma^2} \tag{2.14}$$

Clearly the critical crack length below which the crack would remain stable decreases quickly with stress level. Alternatively, the critical stress level that a cracked body can sustain is

$$\sigma_c = \sqrt{2E\gamma / \pi a} \tag{2.15}$$

for constant load under plane stress condition.

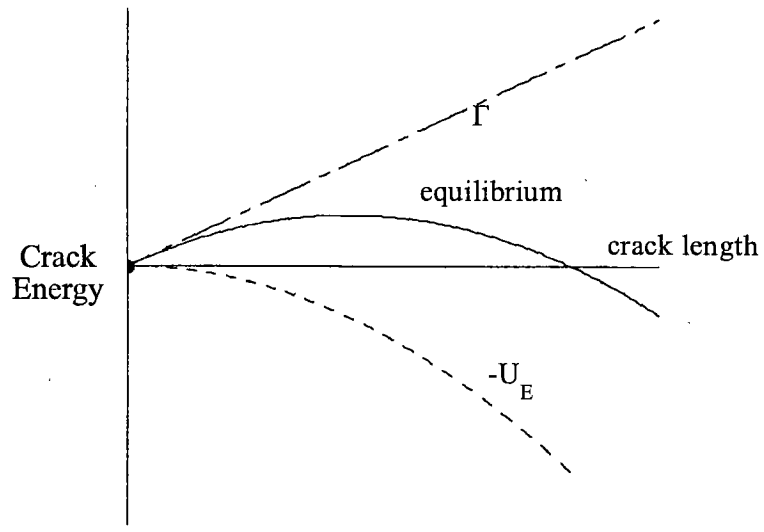

Fig.2.2 Energetics of Griffith crack in uniform tension: linear elastic.

There are two important implications of equation (2.15). Firstly, the critical stress level for a given crack length varies with materials, viz some materials (with high surface energy) are tougher than others. Secondly, the critical stress level decreases with crack length, ie the larger the crack, the easier it may become unstable.

The physical meaning of the energy release rate G is that it characterises the amount of energy that would be released if the crack advances a unit length. When this value is greater than the surface energy of the material, then crack growth would occur, otherwise, no crack propagation would be possible. It should be pointed out that equation (2.9) is correct only when the cracked body behaves linearly; if the object is nonlinear elastic or considerable plasticity occurs, equation (2.8) is no longer valid and hence the original equation (2.6) should be used instead. A graphical illustration is shown in Fig. 2.3. For linear elastic problem, the potential energy $\Pi = U_E - W$ is equal to the area of the triangle (but opposite in sign), incidentally it is also equal to the strain energy in this instance. If the elastic body is nonlinear, like rubber, Π is equal to the upper hatched area, while U_E is actually equal to the area below the load-deflection curve.

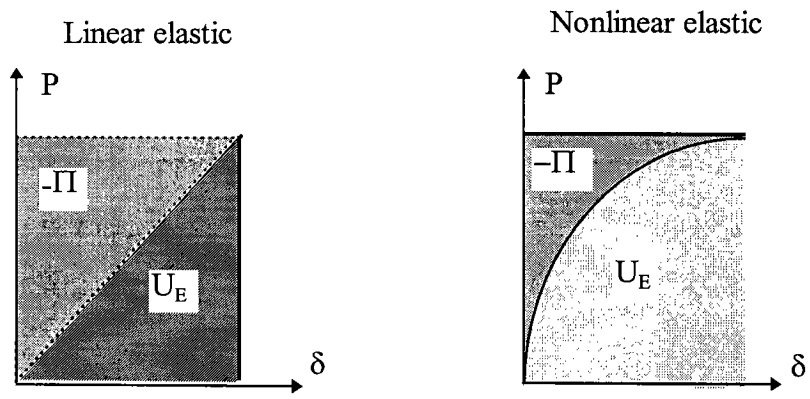

Fig. 2.3 Potential energy for (a) linear and (b) nonlinear elasticity.

2.3 Energy Release Rate *G* and Compliance

The energy release rate G defined in equation (2.9) provides a powerful tool for studying fracture problems of cracked bodies from a global view. The energy release rate is sometimes referred to as the rate of strain energy flux flowing toward a crack tip as the crack extends.

Let us consider the load displacement curve for a cracked specimen made of *linear elastic* media as shown in Fig.2.4. When the crack has length a, the specimen is less compliant than when the crack has length $a+\delta a$. The compliance C of the specimen is the displacement per unit load, i.e the reciprocal of stiffness. In general we may write

$$C = \frac{u}{P} \tag{2.16}$$

which is a geometry constant, dependent on crack length and dimensions of the body. Here the displacement u refers to the relative displacement measured between the loading points; see Fig. 2.4. A cracked body may be subjected to loads or displacement, or a combination of both. In the following we will consider two extreme cases: constant load (Fig 2.5a) and constant displacement or 'fixed grip' condition (Fig.2.5b), separately.

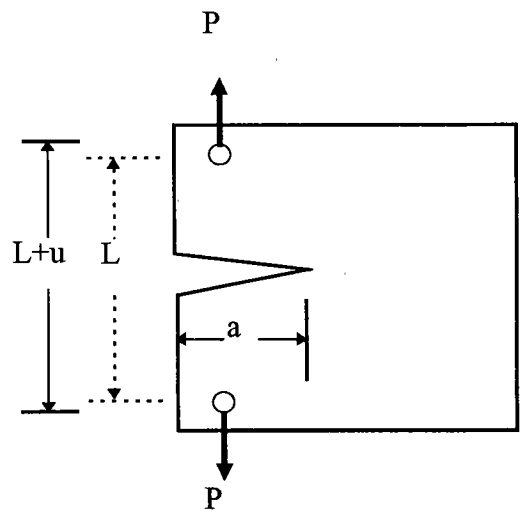

Fig.2.4 Geometry of an edge cracked plate under tension

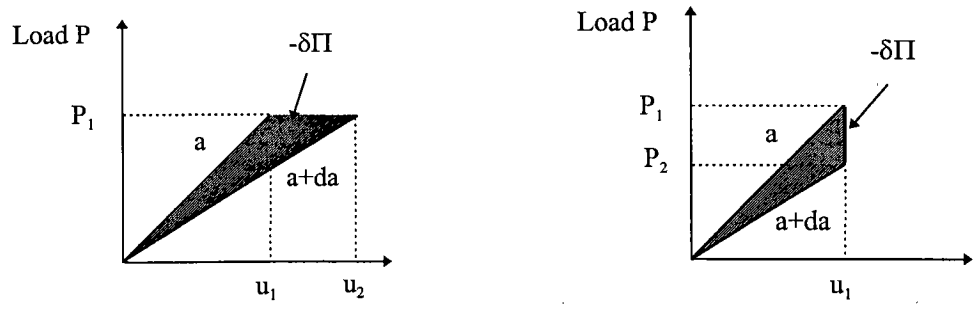

Fig 2.5 Load displacement characteristics for cracked bodies: (a) constant load crack extension, (b) crack extension under constant displacement.

2.3.1 Constant Load Conditions

As discussed previously, the potential energy in the specimen is the area above the load-displacement curve (the area below the load versus displacement curve is the strain energy stored in the specimen while the area of the rectangle is the work done by external force). The potential energy change $\delta\Pi$ is the difference between the external work done and the stored but recoverable elastic strain energy. The energy stored in the specimen for a crack of length $a+\delta a$ is greater than in the situation when the crack was length a, the increase being

$$\delta U_E = \frac{1}{2} P_1 u_2 - \frac{1}{2} P_1 u_1 \tag{2.17}$$

However, to attain this stored energy the load has moved a distance u_2-u_1 and so the work done by the external applied load is

$$\delta W = P_1(u_2 - u_1) \tag{2.18}$$

Clearly the elastic energy stored in the system which could be released back to the environment after crack extension is less than the work done by the applied loads. The amount of the energy that appears to have 'vanished' is equal to

$$-\delta\Pi = \delta W - \delta U_E = P_1(u_2 - u_1) - \frac{1}{2} P_1(u_2 - u_1) = \frac{1}{2} P_1(u_2 - u_1) = \frac{1}{2} P_1 \delta u \tag{2.19}$$

which is the hatched area in Fig. 2.4(a), equal to the energy spent in increasing crack surfaces. In this case, the energy required for crack extension is not supplied by the existing strain energy stored in the system, but the work performed by the external loads; the elastic energy of the solid is actually increased. Thus the term "strain energy release rate" in this case is physically inappropriate. A better name should be "potential energy release rate".

2.3.2 Constant Displacement Condition

Similarly, under fixed grip condition, an increase in crack length causes a decrease in stored elastic strain energy given by

$$\delta U_E = \frac{1}{2}(P_1 - P_2)u_1 = \frac{1}{2}u_1 \delta P \tag{2.20}$$

which is the hatched area in Fig.2.4(b). Since no external work is done, the above energy is that spent in increasing crack surfaces.

2.3.3 Determination Of Energy Release Rate From Compliance

To summarise the above results for constant load and constant displacement,

- the constant load condition requires a potential energy release rate of $\frac{1}{2}P\delta u$.
- the fixed-grip condition requires a potential energy release of $\frac{1}{2}u\delta P$.

In mathematical terms as δA tends to zero we can say that the compliance of C is the same for both cases, which is the same as stating that the difference between the two shaded areas of Fig.2.5 tends to zero. In other words, $\delta u = C\delta P$, and the release of energy for crack extension in both cases is given by

$$\frac{1}{2}CP\delta P \tag{2.21}$$

Therefore the strain (or potential) energy release rate (with respect to crack length) for small crack extension δA can, therefore, be found experimentally in a plate of uniform thickness B as

$$G = \frac{P}{2}\frac{\delta u}{\delta A} = \frac{P^2}{2}\frac{\delta C}{\delta A} \tag{2.22}$$

Thus by taking measurements of the compliance of a specimen with different crack lengths, it is possible to determine δC/δa for a given crack length and so determine G. Note $A = a \cdot B$ when there is only one crack tip (e.g. edge cracked component) and $A = 2a \cdot B$ for centre cracked system. However, it is important to note that the strain energy release rate is identical for constant load and constant displacement conditions. As indicated by equation (2.22), the strain energy release for a given applied load is proportional to the differentiative of the compliance with respect to crack length, independent of loading condition.

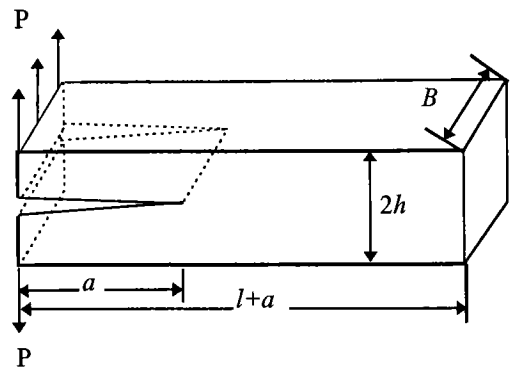

Fig. 2.6 Double cantilever beam

Example 2.1 For a double cantilever beam (DCB) with $a>>2h$ and $l>>2h$, as shown in Fig.2.6, determine the strain energy release rate G.

Solution

The two arms of the DCB may be considered to a first approximation as cantilevers.

Method 1: The displacement at the loading point is

$$u = \frac{Pa^3}{3EI} \quad \text{where} \quad I = \frac{Bh^3}{12}$$

hence the relative displacement of the two points of load application is

$$v = 2u = \frac{8Pa^3}{EBh^3}$$

thus the compliance of the specimen is

$$C = \frac{v}{P} = \frac{8a^3}{EBh^3}$$

It follows that the energy release rate G is

$$G = \frac{P^2}{2B}\frac{\partial C}{\partial a} = \frac{12P^2a^2}{EB^2h^3}$$

Method 2: The strain energy stored in the cantilever beam specimen can be easily obtained by integration,

$$U_E = 2\int_0^a \frac{M^2(x)}{2EI}dx$$

according to equation (2.9) the energy release rate is

$$G = \frac{\partial U_E}{\partial A} = \frac{\partial U_E}{B\partial a} = \frac{M^2(x=a)}{EBI} = \frac{P^2a^2}{EBI} = \frac{12P^2a^2}{EB^2h^3}$$

Example 2.2 Determine the energy release rate for a end notched flexure (ENF) component, shown in Fig.2.7, which is adhesively bonded.

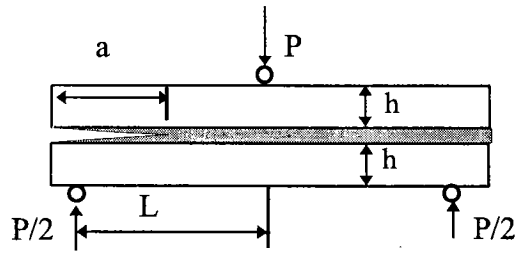

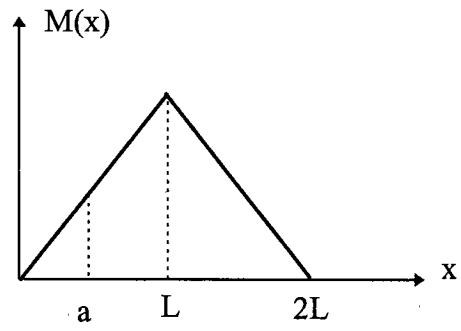

Fig.2.7 End notched flexure specimen and bending moment diagram.

Solution Similar to the previous example, the strain energy stored in the component is

$$U_E = 2\int_0^a \frac{(\frac{1}{2}M_1)^2}{2EI_1}dx + \int_a^L \frac{M_1^2(x)}{2EI_2}dx + \int_L^{2L} \frac{M_2^2(x)}{2EI_2}dx$$

where E is the Young's modulus of the plate and

$$M_1(x) = \frac{Px}{2} \quad I_1 = \frac{Bh^3}{12}$$

$$M_2(x) = PL - \frac{Px}{2} \qquad I_2 = \frac{B(2h)^3}{12} = \frac{8Bh^3}{12}$$

so

$$U_E = \int_0^a \frac{12P^2x^2}{16EBh^3}dx + \int_a^L \frac{12P^2x^2}{64EBh^3}dx + \int_L^{2L} \frac{M_2^2(x)}{2EI_2}dx$$

hence the energy release rate is

$$G = \frac{\partial U_E}{\partial A} = \frac{\partial U_E}{B\partial a} = \frac{3P^2a^2}{4EB^2h^3} - \frac{3P^2a^2}{16EB^2h^3} = \frac{9P^2a^2}{16EB^2h^3}$$

Example 2.3 Determine the energy release rate for a cracked lap shear (CLS) specimen (see Fig.2.8).

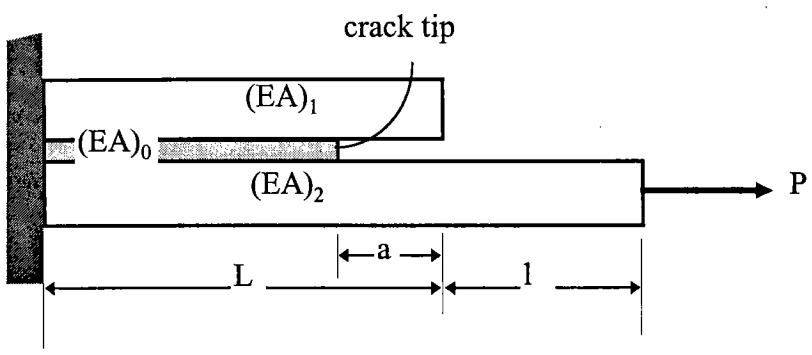

Fig.2.8 Adhesively bonded cracked lap shear specimen

Solution Assuming the bending deflection of the overhang region does not contribute to the strain energy, the strain energy stored in the system is

$$U_E = \int_0^{L-a} \frac{P^2}{2(EA)_0}dx + \int_{L-a}^{L+l} \frac{P^2}{2(EA)_2}dx$$

thus the energy release rate is

$$G = \frac{\partial U_E}{\partial A} = \frac{\partial U_E}{B\partial a} = \frac{1}{B}\left[-\frac{P^2}{2(E_1t_1 + E_2t_2)B} + \frac{P^2}{2E_2t_2B}\right] = \frac{P^2}{2B^2}\frac{E_1t_1}{E_1t_1 + E_2t_2}$$

It is interesting to note that, unlike the previous example, the energy release rate for a cracked lap shear specimen is independent of crack length. This feature offers a convenient method in determining the critical energy release rate, as the precise location of the crack tip is not important.

It should be pointed that the above method applies only when the entire system, including adhesive, is elastic. When the adhesive yields, a rather more complicated analysis using elasto-plastic fracture mechanics is required. Furthermore, the local bending effect due to load eccentricity is ignored in the present analysis. In reality, when the overhang length, *l*, is sufficiently long, geometrically nonlinear deformation

would occur, which will induce a local peel stress at the crack tip, hence a mode I fracture component.

2.4 Stress Intensity Factor *K*

Before proceeding to consider the stress analysis of cracked bodies, it is important to distinguish basic 'modes' of stressing. As shown in Fig.2.9, the three basic modes are: opening (mode I), in-plane shear (mode II) and out-of-plane tearing (mode III). Mode I corresponds to normal separation of the crack faces under the action of tensile stresses, which is by far the most widely encountered in practice. The difference between Mode II and Mode III is that the shearing action in the former case is normal to the crack front in the plane of the crack whereas the shearing action in Mode III is parallel to the crack front. A cracked body in reality can be loaded in any one of these three, or a combination of these three modes.

By means of various techniques, the stress, strain, and displacement fields associated with a crack embedded in an elastic solid can be solved analytically. One of such method is due to Westergaard, who introduced the following stress function,

$$\Phi = \mathrm{Re}\,\overline{\overline{Z}} + y\,\mathrm{Im}\,\overline{Z} \tag{2.23}$$

where $Z=Z(z)$ is an analytical function of the complex variable $z=x+iy$. Here $\overline{Z} = \int Z(z)dz$ and $\overline{\overline{Z}} = \int\int Z(z)dzdz$. The semi-inverse solution (mainly by trial-and-error) for a crack in an infinite plate subjected to a remote stress σ is

$$Z(z) = \frac{\sigma}{\sqrt{1-(a/z)^2}} \tag{2.24a}$$

Note the origin of the coordinate is at the center of the crack. By transforming the origin to the right-hand crack tip, i.e., $z = a + re^{-i\theta}$, all the stress components can be derived. In the limit of small enough values of *r/a*, equation (2.24a) can be expressed as

$$Z = \frac{\sigma\sqrt{a}}{\sqrt{2r}} e^{-i\theta/2} \tag{2.25b}$$

From differentiation of equation (2.24a),

$$Z'(z) = \frac{-\sigma a^2}{\left(z^2-a^2\right)^{3/2}} \tag{2.26c}$$

hence

$$Z' = \frac{\sigma a}{2r} e^{-3i\theta/2} \tag{2.27d}$$

For the configuration shown in Fig.2.10, the stresses can be expressed in a simple form, noting equation (1.14),

$$\sigma_{ij} = \frac{K}{\sqrt{2\pi r}} f_{ij}(\theta) \tag{2.28a}$$

and displacement

$$u_i = \frac{K}{2\mu}\sqrt{\frac{r}{2\pi}} g(\theta) \tag{2.25b}$$

where the K terms are the stress-intensity factors which embody the loading and geometry conditions. A complete list of the stress and displacement fields for three fracture modes is given in Table 2.1. The corresponding formulae for polar coordinates are given in Table 2.2.

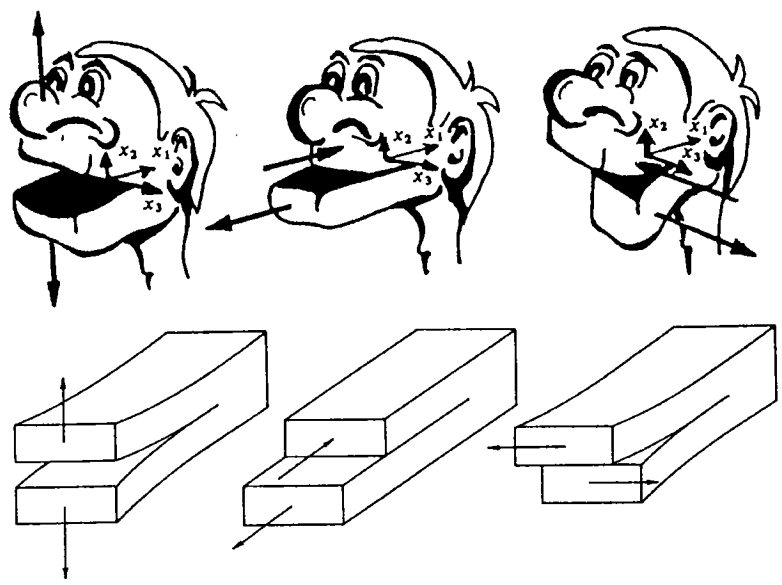

Fig.2.9 Basic modes of crack extension; (a) opening mode, (b) sliding mode, and (c) tearing mode.

The relative displacement between crack faces at position x is given by

$$u_y = \frac{2K}{E}\sqrt{\frac{a^2 - x^2}{\pi a}} \tag{2. 29}$$

for plane stress condition. Clearly the maximum crack opening occurs at the centre of the crack, equal to $\frac{2K}{E}\sqrt{\frac{a}{\pi}}$. The stress distribution ahead of the crack tip, not necessarily near crack tip, is

$$\sigma_{yy} = \frac{\sigma(a+r)}{\sqrt{2ar+r^2}} \tag{2.30}$$

$$\sigma_{xx} = \frac{\sigma(a+r)}{\sqrt{2ar+r^2}} - \sigma \tag{2.31}$$

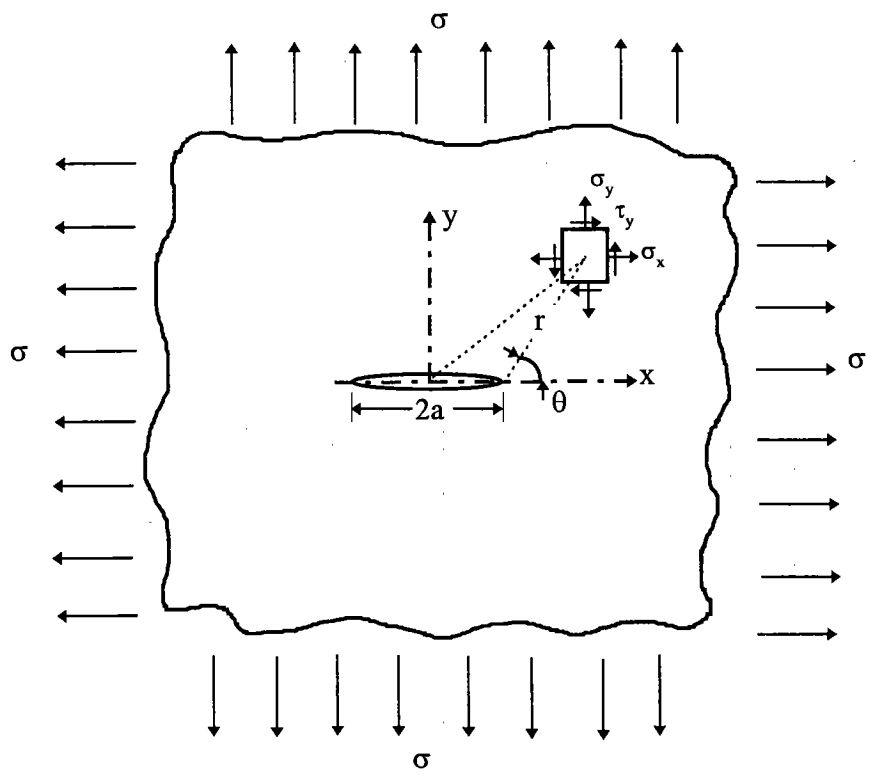

Fig.2.10 A crack of length 2a *in an infinite plate*

Example 2.4 Estimate the relative size of the singularity dominated zone ahead of a through crack in an infinite plate subjected to remote uniaxial tension.

Solution Equations (2.27) and (2.28) can be rewritten as

$$\sigma_{yy} = \frac{K}{\sqrt{2\pi r}} \frac{(1+r/a)\sqrt{2r/a}}{\sqrt{2r/a+(r/a)^2}}$$

and

$$\sigma_{xx} = \frac{K}{\sqrt{2\pi r}} \left(\frac{(1+r/a)\sqrt{2r/a}}{\sqrt{2r/a+(r/a)^2}} - \sqrt{2r/a} \right)$$

Clearly the actual stress normal to the crack plane σ_{yy} is higher than that given by equation (2.25a). Hence the singular solution is valid only near the crack tip; we define this as *the singularity dominated zone*, as shown in Fig.2.11. The size of this zone can be estimated by considering the ratio of the actual stress on the crack plane to the singularity limit. This is depicted in Fig.2.12. Note that the stress in the y direction is close to the singularity limit for relatively large distances from the crack tip, but the x stress diverges considerably from the near-tip limit. Let us arbitrarily define the singularity zone as the region within which the deviation is less than 20% for the x stress; this represents a value of r/a=0.02. In other words, the term "singularity zone" is approximately one-fiftieth of the half crack size.

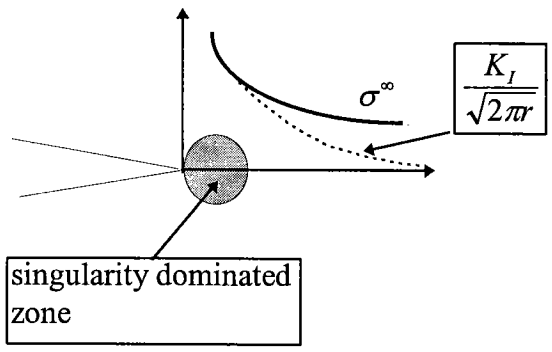

Fig.2.11 Distribution of the stress normal to the crack plane

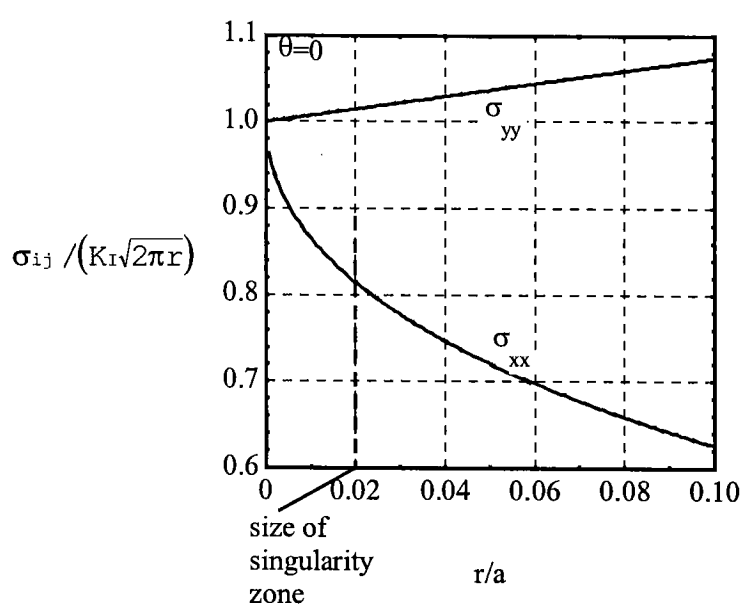

Fig.2.12 Ratio of actual stresses on the crack plane to the singularity limit

Table 2.1 Stress and displacement fields ahead a crack tip for modes I, II, III

	Mode I	Mode II	Mode III
σ_{xx}	$\frac{K_I}{\sqrt{2\pi r}}\cos\frac{\theta}{2}\left[1-\sin\frac{\theta}{2}\sin\frac{3\theta}{2}\right]$	$-\frac{K_{II}}{\sqrt{2\pi r}}\sin\frac{\theta}{2}\left[2+\cos\frac{\theta}{2}\cos\frac{3\theta}{2}\right]$	0
σ_{yy}	$\frac{K_I}{\sqrt{2\pi r}}\cos\frac{\theta}{2}\left[1+\sin\frac{\theta}{2}\sin\frac{3\theta}{2}\right]$	$\frac{K_{II}}{\sqrt{2\pi r}}\sin\frac{\theta}{2}\cos\frac{\theta}{2}\cos\frac{3\theta}{2}$	0
τ_{xy}	$\frac{K_I}{\sqrt{2\pi r}}\cos\frac{\theta}{2}\sin\frac{\theta}{2}\cos\frac{3\theta}{2}$	$\frac{K_{II}}{\sqrt{2\pi r}}\cos\frac{\theta}{2}\left[1-\sin\frac{\theta}{2}\sin\frac{3\theta}{2}\right]$	0
σ_{zz}	$\begin{cases}0 & \text{plane stress}\\ \nu(\sigma_{xx}+\sigma_{yy}) & \text{plane strain}\end{cases}$	$\begin{cases}0 & \text{plane stress}\\ \nu(\sigma_{xx}+\sigma_{yy}) & \text{plane strain}\end{cases}$	0
τ_{xz}	0	0	$-\frac{K_{III}}{\sqrt{2\pi r}}\sin\frac{\theta}{2}$
τ_{yz}	0	0	$\frac{K_{III}}{\sqrt{2\pi r}}\cos\frac{\theta}{2}$
u_x	$\frac{K_I}{2\mu}\sqrt{\frac{r}{2\pi}}\cos\frac{\theta}{2}\left[\kappa-1+2\sin^2\frac{\theta}{2}\right]$	$\frac{K_{II}}{2\mu}\sqrt{\frac{r}{2\pi}}\sin\frac{\theta}{2}\left[\kappa+1+2\cos^2\frac{\theta}{2}\right]$	0
u_y	$\frac{K_I}{2\mu}\sqrt{\frac{r}{2\pi}}\sin\frac{\theta}{2}\left[\kappa+1-2\cos^2\frac{\theta}{2}\right]$	$\frac{K_{II}}{2\mu}\sqrt{\frac{r}{2\pi}}\cos\frac{\theta}{2}\left[\kappa-1-2\sin^2\frac{\theta}{2}\right]$	0
u_z	$-\frac{\nu z}{E}(\sigma_{xx}+\sigma_{yy})$ plane stress 0 plane strain	$-\frac{\nu z}{E}(\sigma_{xx}+\sigma_{yy})$ plane stress 0 plane strain	$\frac{K_{III}}{\mu}\sqrt{\frac{r}{2\pi}}\sin\frac{\theta}{2}$

μ is the shear modulus, κ=3-4ν for plane strain and κ=(3-ν)/(1+ν) for plane stress

It is easy to show that the principal stresses for mode I are

$$\sigma_1 = \frac{K_I}{\sqrt{2\pi r}}\cos\frac{\theta}{2}\left(1+\sin\frac{\theta}{2}\right) \tag{2.32}$$

$$\sigma_2 = \frac{K_I}{\sqrt{2\pi r}}\cos\frac{\theta}{2}\left(1-\sin\frac{\theta}{2}\right) \tag{2.33}$$

Table 2.2 Stress fields ahead a crack tip in a polar coordinate system

	Mode I	Mode II	Mode III
σ_{rr}	$\frac{K_I}{\sqrt{2\pi r}}\cos\frac{\theta}{2}\left[1+\sin^2\left(\frac{\theta}{2}\right)\right]$	$\frac{K_{II}}{\sqrt{2\pi r}}\sin\frac{\theta}{2}\left[1-3\sin^2\left(\frac{\theta}{2}\right)\right]$	0
$\sigma_{\theta\theta}$	$\frac{K_I}{\sqrt{2\pi r}}\cos^3\left(\frac{\theta}{2}\right)$	$-\frac{3K_{II}}{\sqrt{2\pi r}}\sin\frac{\theta}{2}\cos^2\left(\frac{\theta}{2}\right)$	0
$\tau_{r\theta}$	$\frac{K_I}{\sqrt{2\pi r}}\sin\frac{\theta}{2}\cos^2\left(\frac{\theta}{2}\right)$	$\frac{K_{II}}{\sqrt{2\pi r}}\cos\frac{\theta}{2}\left[1-3\sin^2\left(\frac{\theta}{2}\right)\right]$	0
τ_{xz}	0	0	$\frac{K_{III}}{\sqrt{2\pi r}}\sin\frac{\theta}{2}$
τ_{yz}	0	0	$\frac{K_{III}}{\sqrt{2\pi r}}\cos\frac{\theta}{2}$

In general the stress intensity factor depends on the applied stress, crack size, and the geometry,

$$K = Y\sigma\sqrt{\pi a} \tag{2.34}$$

where Y is called the geometry factor, signifying the geometry of a crack system in relation to the applied load. Normally this geometry factor can be looked up in technical reference books. For a centre crack in an infinite plate, $Y = 1.0$. The geometry of the cracked body imposes an effect on the new crack tip stress field, thus modifying the value of the stress intensity factor. In general, if the edge crack is situated in a strip of finite width, w, then the correction factor becomes a function of (a/w)

$$Y = f(a / w) \tag{2.35}$$

The simplest geometry factor is that for an edge crack of length, a, at the edge of a semi-infinite half space: the increased ability of the crack to open causes the stress intensity factor to increase by some 12%,

$$K_I = 1.12\,\sigma\sqrt{\pi a} \tag{2.36}$$

The determination of this geometry term is a problem of stress analysis. Any realistic geometry requires recourse to numerical methods, as very few closed form solutions exist. The most popular and efficient method is finite element analysis. Other techniques include experimental and semi-theoretical; more will be said about this later. Table 2.3 lists stress intensity factors and the geometry factors for a number of practical configurations. A more comprehensive list could be found in a two-volume handbook (Murakami, 1987).

Table 2.3 Stress intensity factors

Geometry	Stress Intensity Factor
1. Crack in an infinite body 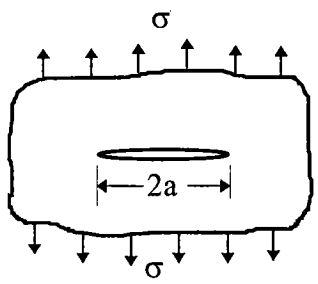	$K_I = \sigma\sqrt{\pi a}$
2. Centre crack in a strip of finite width 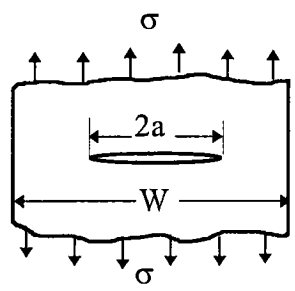	$K_I = \sqrt{\sec\frac{\pi a}{W}}\sigma\sqrt{\pi a}$
3. Edge crack in a semi-infinite body 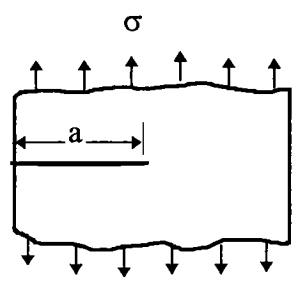	$K_I = 1.12\sigma\sqrt{\pi a}$
4. Centre crack in a finite width strip 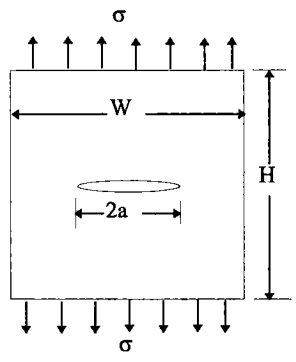	$K_I = f\left(\frac{a}{W}\right)\sigma\sqrt{\pi a}$

a/W	f(a/W)	
	h/W=1.0	h/W=∞
0	1.12	1.12
0.2	1.37	1.21
0.4	2.11	1.35
0.5	2.83	1.46

5. Edge crack in a beam of width B subjected to bending

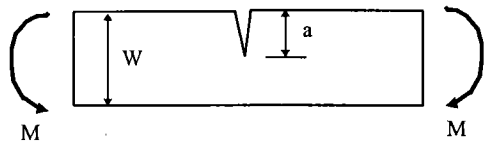

$$K_I = f\left(\frac{a}{W}\right)\sigma\sqrt{\pi a} \quad \text{where} \quad \sigma = \frac{6M}{BW^2}$$

a/W	$f(a/W)$
0.1	1.044
0.2	1.055
0.3	1.125
0.4	1.257
0.5	1.500
0.6	1.915

6. Thin-section (plane stress) double split beam

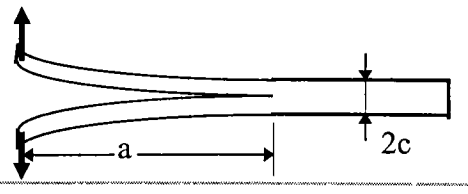

$$K_I = 2\sqrt{3}\frac{Pa}{c^{3/2}}$$

7. Circumferentially notched rod

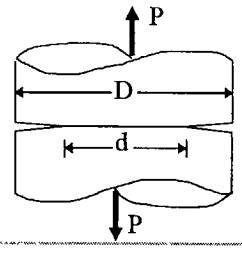

$$K_I = \frac{0.932P\sqrt{D}}{\sqrt{\pi d^2}} \quad \text{for} \quad 1.2 \le \frac{D}{d} < 2.1$$

8. Compact tension specimen (CST)

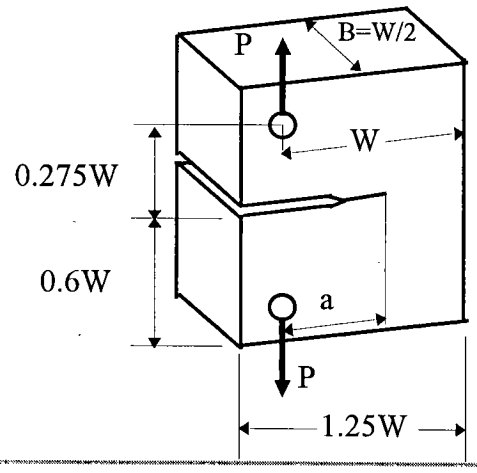

$$K_I = Y\frac{P\sqrt{\pi}}{B\sqrt{W}}$$

$$Y = 16.7\left(\frac{a}{W}\right)^{1/2} - 104.7\left(\frac{a}{W}\right)^{3/2} + 369.9\left(\frac{a}{W}\right)^{5/2} - 573.8\left(\frac{a}{W}\right)^{7/2} + 360.5\left(\frac{a}{W}\right)^{9/2}$$

9. Single-edge notch bend (SENB), thickness B

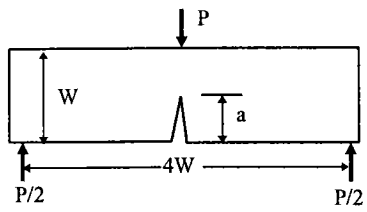

$B = W / 2$

$$K_I = Y \frac{4P\sqrt{\pi}}{B\sqrt{W}}$$

$$Y = 1.63\left(\frac{a}{W}\right)^{1/2} - 2.6\left(\frac{a}{W}\right)^{3/2} + 12.3\left(\frac{a}{W}\right)^{5/2} - 21.3\left(\frac{a}{W}\right)^{7/2} + 21.9\left(\frac{a}{W}\right)^{9/2}$$

10. Crack emanating from a hole in an infinite body

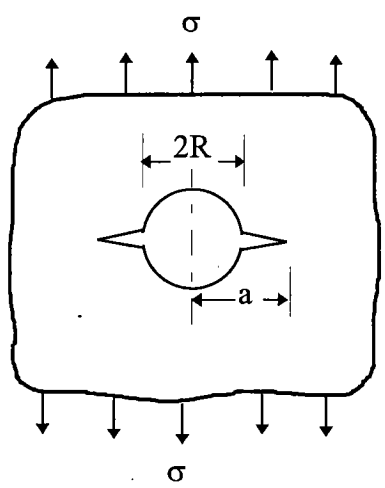

$$K_I = f\left(\frac{a}{R}\right)\sigma\sqrt{\pi a}$$

a/R	$f(a/R)$
1.01	0.3256
1.02	0.4514
1.04	0.6082
1.06	0.7104
1.08	0.7843
1.10	0.8400
1.20	0.9851
1.25	1.0168
1.30	1.0358
1.40	1.0536
1.80	1.0495

A few points of interest arise from these solutions. Firstly, the stress intensity factor defines the amplitude of the crack tip singularity, and consequently the intensity of the local stress field. Local stresses near the crack tip are proportional to K, which uniquely defines the crack tip conditions. This single-parameter description of crack tip conditions is probably the most important concept of fracture mechanics. Secondly, it should be pointed that these solutions are valid only in the vicinity of the crack tip; higher order terms need to be taken into account when far field information is required.

2.5 Superposition Method

Since the stresses and displacements are linearly proportional to the stress intensity factor, it follows that the superposition principle also applies to crack problems. This provides a very important tool for applying fracture mechanics to practical problems

with the aid of handbooks. The underlying principle is that stresses induced by various loads can be added together. It should be pointed that the superposition method applies only to cases where a structure is subjected to various loads but of the same mode. For example, the crack tip stresses for a cracked component under combined tension and bending are,

$$\sigma_{ij} = \frac{K_I^{tension}}{\sqrt{2\pi r}} f_{ij}(\theta) + \frac{K_I^{bending}}{\sqrt{2\pi r}} f_{ij}(\theta) \tag{2.37}$$

Because the angular function $f_{ij}(\theta)$ is the same for the same fracture mode, the above equation can be rewritten as

$$\sigma_{ij} = \frac{K_I^{total}}{\sqrt{2\pi r}} f_{ij}(\theta) \tag{2.38}$$

where

$$K_I^{total} = K_I^{tension} + K_I^{bending} \tag{2.39}$$

In general, the stress intensity factor for a combination of load systems A, B, C can be obtained simply by superposition

$$K_I = K_I^A + K_I^B + K_I^C \tag{2.40}$$

and similarly for modes II and III.

Example 2.5 Determine the stress intensity factor for a edge cracked plate subjected to a combined tension and bending.

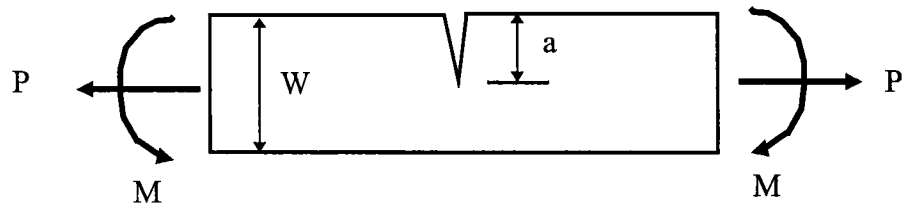

Fig.2.13 An edge cracked plate under tension and bending

Solution

From Table 2.3, the stress intensity factor caused by the bending (case 5) is

$$K^{(M)} = f_M\left(\frac{a}{W}\right)\frac{6M}{BW^2}\sqrt{\pi a}$$

The stress intensity factor for the tension load (case 4) is

$$K^{(P)} = f_P\left(\frac{a}{W}\right)\frac{P}{BW}\sqrt{\pi a}$$

Thus the total stress intensity factor is

$$K = \sqrt{\pi a}\left(\frac{P}{BW}f_P\left(\frac{a}{W}\right) + \frac{6M}{BW^2}f_M\left(\frac{a}{W}\right)\right)$$

For a ratio a/W=0.2, we have $K = \sqrt{\pi a}\left(1.21\frac{P}{BW} + 1.055\frac{6M}{BW^2}\right)$.

Example 2.6 Consider a symmetric case of two very small cracks at a circular hole (See Fig.2.14(a)) along the x-axis in a wide plate subjected to uniaxial tension σ along the y-axis. Determine the stress intensity factor.

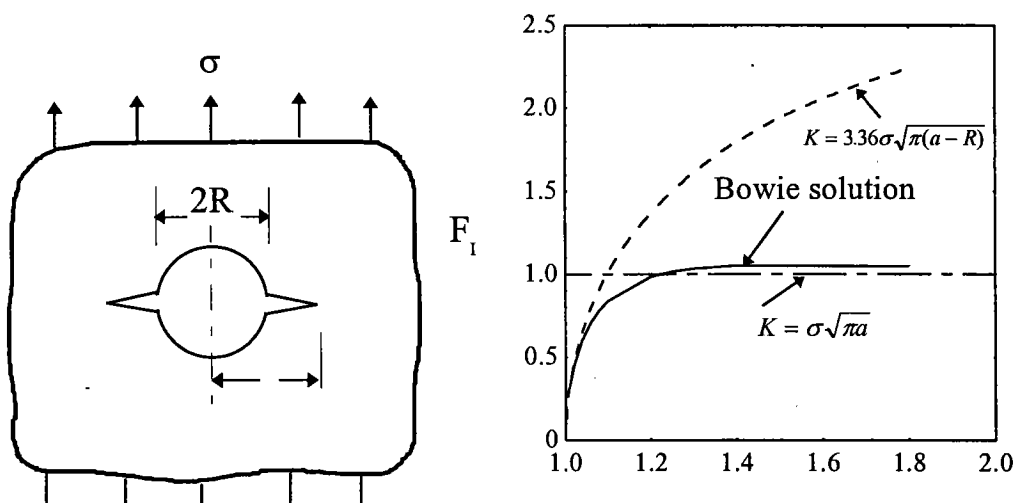

Fig.2.14 Stress intensity factor correction factor for a crack emanating from a hole.
(a) Two symmetrical cracks emanating from a circular hole and
(b) the stress intensity factor.

Solution Due to the stress concentration near the circular hole (K_t=3) an element at the rim of the hole is subjected to a tensile stress 3σ along the y-axis. By the principal of superposition and for a small crack length, we have

$$K_I = 1.12(3\sigma)\sqrt{\pi(a-R)} = 3.36\sigma\sqrt{\pi a}\sqrt{1-\frac{R}{a}} = 3.36\sqrt{1-\frac{1}{a/R}}\sigma\sqrt{\pi a}$$

which is shown in Fig.2.14 together with the numerical solution obtained by Bowie (1956).

Clearly for very short cracks the above approximation is very close to the numerical solution. For long cracks (crack length $a >> R$), we may assume as an engineering approach that the combination behaves as if the hole were part of the crack, hence $K = \sigma\sqrt{\pi a}$. As shown in Fig.2.14, these two asymptotic solutions provide two bounds to the actual solution.

2.6 Relationship Between *G* and *K*

We can now return to the Griffith's energy concept, with special reference to its relation to the stress intensity factor. Proceeding as before, we may identify the mechanical energy release during the crack extension with the work done by hypothetically imposed surface tractions. As illustrated in Fig. 2.15, forces are applied to the crack edge, sufficient to close the crack over an infinitesimal distance. The work done by this force is obviously equal to the amount of energy that needs to be consumed in order to make the crack grow by this distance.

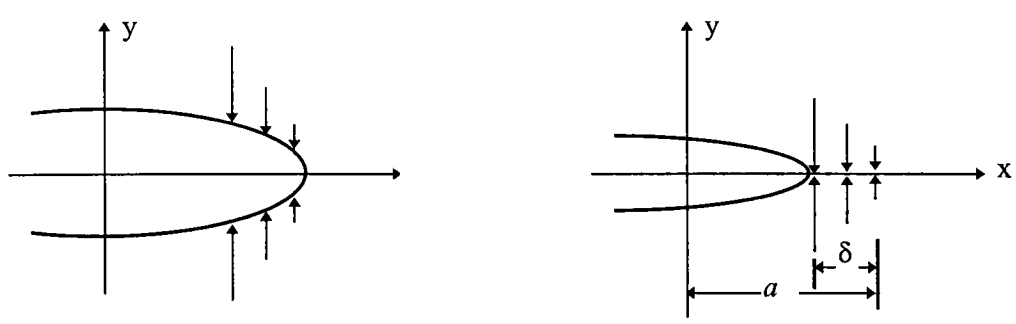

Fig. 2.15 Calculation of strain energy release rate

Thus the strain-energy release for a crack growth of δ may be expressed as

$$\delta U_E = 2B\int_0^{\delta} \tfrac{1}{2}\sigma_y u_y dx = 2B\int_{a-\delta}^{a} \tfrac{1}{2}\sigma_y u_y dx \tag{2.41}$$

where the factor 2 arises because the crack has two opposing crack surfaces, and the factor $\frac{1}{2}$ is because of the assumed proportionality between tractions and the corresponding displacement. The thickness of the plate is denoted as B. After substituting the expressions for σ_y and u_y (see Table 3.1), the integration of equation (2.34) leads to

$$\begin{aligned} G &= \lim_{\delta\to 0}\frac{2K_I^{\,2}}{\pi E\delta}\int_0^{\delta}\sqrt{\frac{\delta-r}{r}}dr = \frac{2K_I^{\,2}}{\pi E}\int_0^{\pi/2}\sqrt{\frac{\cos^2\phi}{\sin^2\phi}}2\delta\sin\phi\cos\phi d\phi \\ &= \frac{K_I^{\,2}}{E} \end{aligned} \tag{2.42}$$

for plane stress. Similarly, for plane strain condition (see Chapter 1)

$$G = (1-\nu^2)\frac{K_I^2}{E} \tag{2.43}$$

It can also be shown for mode II and mode III,

$$G_{II} = (1-\nu^2)\frac{K_{II}^2}{E} \quad \text{and} \quad G_{III} = (1+\nu)\frac{K_{III}^2}{E} \tag{2.44}$$

for plane strain condition.

The total energy release rate in combined mode cracking can be obtained by summing up the energies for different modes:

$$G = G_I + G_{II} + G_{III} = \begin{cases} \dfrac{K_I^2}{E} + \dfrac{K_{II}^2}{E} + \dfrac{K_{III}^2}{E}(1+\nu) & \text{(for plane stress)} \\ (1-\nu^2)\dfrac{K_I^2}{E} + (1-\nu^2)\dfrac{K_{II}^2}{E} + \dfrac{K_{III}^2}{E}(1+\nu) & \text{(for plane strain)} \end{cases} \tag{2.45}$$

However, it is important to note that the derivation of both the stress intensity factor and the strain energy release rate is independent of the actual fracture process hence critical condition of materials. In other words, these only represent the 'driving' force for crack growth and bear no relations to the materials' 'resistance'. This will be discussed in the next chapter.

Example 2.7 For double cantilever beam (DCB) shown in Example 2.2 determine the stress intensity factor K_I using elementary beam theory for applied load P or applied displacement u.

Solution

From the previous analysis, the energy release rate for the cracked system is

$$G = \frac{12P^2a^2}{EB^2h^3}$$

the stress intensity factor is, according to equation (2.40)

$$K = \sqrt{EG/(1-\nu^2)} = \frac{2\sqrt{3}}{\sqrt{1-\nu^2}}\frac{Pa}{Bh^{3/2}}$$

for plane strain condition. Obviously the 'driving' force increases linearly with crack length for a constant applied load. The stress intensity factor can also be expressed in terms of the displacement, u,

$$K = \frac{\sqrt{3}h^{3/2}Eu}{4\sqrt{1-\nu^2}a^2}$$

It should be observed that, under displacement control, the stress intensity factor decreases as the crack extends. Therefore the system is a stable one, in the sense that the crack would stop growing after a certain crack advance unless the displacement is further increased.

Example 2.8 Determine compliance of a centre cracked specimen of width W and crack length 2a. The thickness and height of the specimen are B and H, respectively. The stress intensity factor is given in Table 2.3.

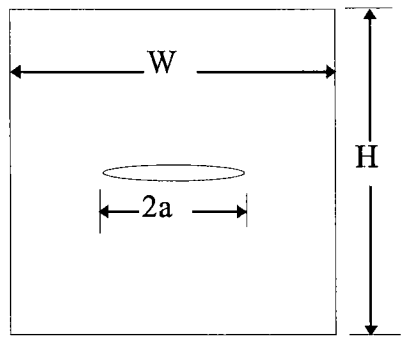

Fig.2.16 A finite centre cracked plate

Solution From Table 2.3 the stress intensity factor is

$$K = \sqrt{\sec\frac{\pi a}{W}}\sigma\sqrt{\pi a}$$

Since

$$G = \frac{P^2}{2}\frac{\partial C}{\partial A} = \frac{P^2}{4B}\frac{dC}{da}$$

for centre cracked plate and

$$G = \frac{K^2}{E}$$

we have

$$\left(\frac{dC}{da}\right)_P = \frac{4B}{EP^2}\sigma^2\pi a\sec\frac{\pi a}{W} = \frac{4}{EBW^2}\pi a\sec\left(\frac{\pi a}{W}\right)$$

hence the compliance is

$$C = \int_0^a \frac{4}{EBW}\frac{\pi a}{W}\sec\left(\frac{\pi a}{W}\right)da + C_0$$

where constant C_0 represents the compliance of the specimen without crack, that is

$$C_0 = \frac{\Delta}{P} = \frac{\varepsilon H}{\sigma BW} = \frac{H}{EBW}$$

To facilitate the integration, we adopt the following approximation

$$\frac{\pi a}{W}\sec\left(\frac{\pi a}{W}\right) = \tan\left(\frac{\pi a}{W}\right)\frac{\frac{\pi}{W}a}{\sin\left(\frac{\pi a}{W}\right)} \approx \tan\left(\frac{\pi a}{W}\right)$$

For comparison, two ratio between the two functions are shown in Fig.2.17. It is seen that the error is less than 10 percent up to a ratio $2a/W$=0.5.

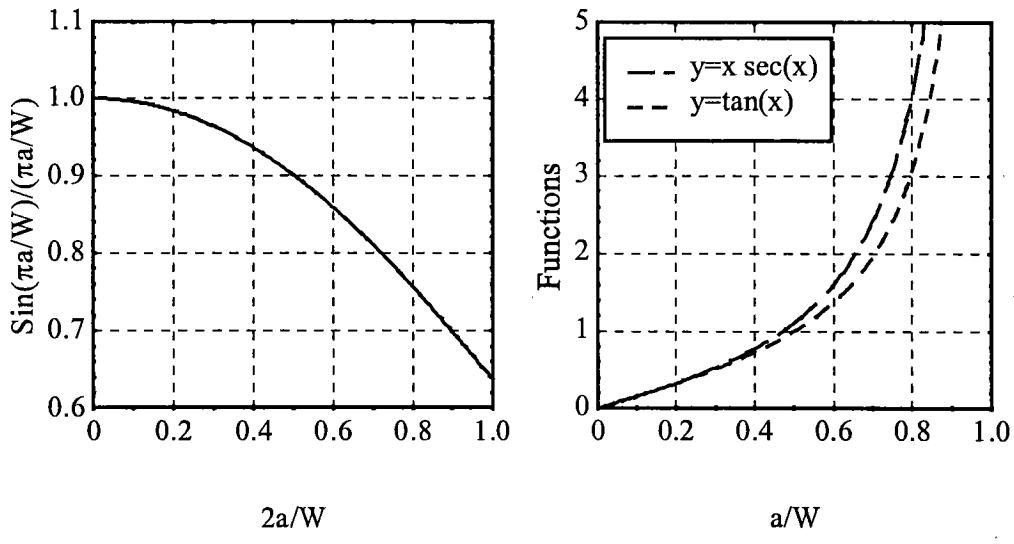

Fig.2.17 Approximations to hyperbolic function $x\sec(x)$ *by* $\tan x$

Now the compliance can be expressed as

$$C = -\frac{4}{EB\pi}\ln\left(\cos\frac{\pi a}{W}\right) + \frac{H}{EBW} = \frac{H}{EBW}\left[1 - \frac{W}{H}\frac{4}{\pi}\ln\left(\cos\frac{\pi a}{W}\right)\right]$$

This is graphically shown below. Clearly the compliance of the specimen increases rapidly as the crack length increases.

These two examples demonstrate that the relationship between the energy release rate and stress intensity factor is not only useful in determining the stress intensity factor for a cracked component from compliance measurement or calculation, but also useful in assessing the compliance of a cracked component.

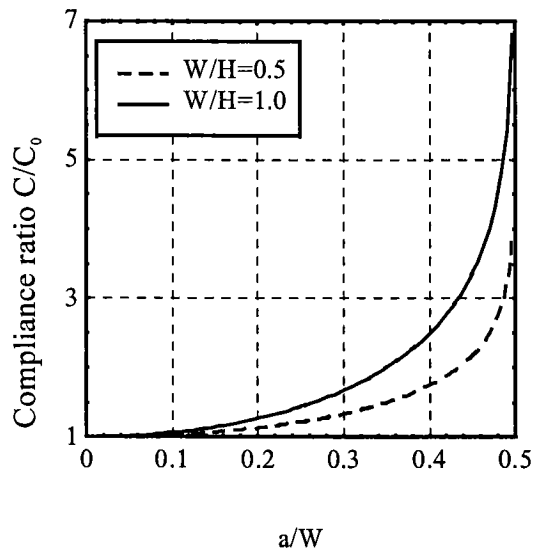

Fig.2.18 Compliance of a centre cracked plate..

3. Plastic Yielding at Crack Tip

In real materials, the theoretically very high elastic stresses in the vicinity of a crack tip exceed the yield strength of the materials. Consequently local plastic yielding will occur. Plastic yielding and the subsequent local elastic-plastic deformation at the tip of a crack plays an extremely important role in the fracture process of materials.

3.1 Irwin's Model

To determine the plastic zone at the crack tip, Irwin presented a simple model assuming the material is elastic-perfectly plastic. Consider the distribution of tensile stress σ_{yy}, acting across a line extending ahead of and in the same direction as the crack. The local y-stress near the crack tip is,

$$\sigma_{yy} = \frac{K_I}{\sqrt{2\pi r}} \tag{3.1}$$

where r is the distance from the crack tip. As a first approximation, we can assume that the boundary between elastic and plastic behaviour occurs when the stress given by the above equation satisfies a yield criterion. For plane stress conditions, yielding occurs when $\sigma_{yy} = \sigma_{ys}$, the uniaxial yield strength of the material. Then the distance ahead of the crack tip over which this happens is

$$r_1 = \frac{K_I^2}{2\pi\sigma_{ys}^2} \tag{3. 2}$$

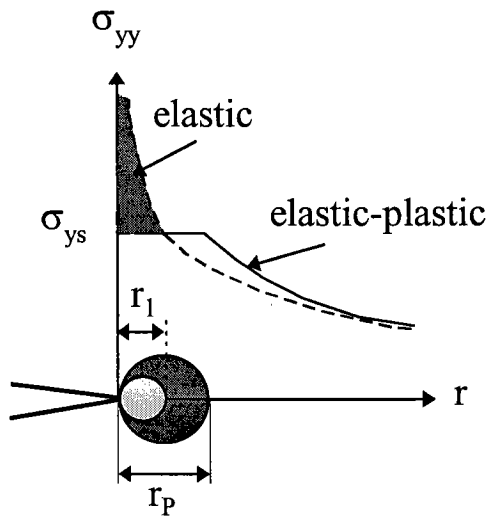

Fig. 3.1 First-order and second-order estimates of plastic zone size

However, when yielding occurs, stresses must redistribute in order to satisfy equilibrium. Since when the elastic stress distribution within the plastic zone is replaced by a constant yield stress, the equilibrium condition along the y direction is violated. The cross-hatched region in Fig. 3.1 represents force that would be present in an elastic material but cannot be carried in the elastic-plastic material because the stress cannot exceed yield. The plastic zone must increase in size in order to accommodate these forces. A simple force balance leads to a second order estimation, assuming the force carried by the elastic stress distribution is the same before and after plastic yielding,

$$\sigma_{ys} r_p = \int_0^{r_1} \sigma_{yy} dr = \int_0^{r_1} \frac{K_I}{\sqrt{2\pi r}} dr \tag{3.3}$$

hence

$$r_p = \frac{1}{\pi}\left(\frac{K_I}{\sigma_{ys}}\right)^2 \tag{3.4}$$

Alternatively, the above result can also be obtained by considering a fictitious crack extending to the centre of the plastic zone, its tip centring at $a + \frac{1}{2} r_p$, where r_p is the size of the plastic zone yet to be determined. Stress distribution directly ahead of the crack is thus

$$\sigma_{yy} = \frac{\sigma\sqrt{\pi(a + r_p/2)}}{\sqrt{2\pi x}} \tag{3.5}$$

Now we assume that the boundary between elastic and plastic regions is given by $\sigma_{yy} = \sigma_{ys}$ at x= $r_p/2$, hence,

$$r_p = a\left(\frac{\sigma}{\sigma_{ys}}\right)^2 \frac{1}{1-\frac{1}{2}\left(\frac{\sigma}{\sigma_{ys}}\right)^2} \approx \frac{1}{\pi}\left(\frac{K_I}{\sigma_{ys}}\right)^2 \tag{3.6}$$

which is the same as equation (3.4). These results need to be modified for plane strain condition; see below.

Example 3.9 Determine the value of K_I where the plane strain plastic zone engulfs the singularity dominated zone.

From Example 2.4 the size of the singularity zone is estimated to be equal to $a/50$. According to equation (3.4) we have

$$\frac{1}{\pi}\left(\frac{K}{\sigma_{ys}}\right)^2 \le \frac{a}{50}$$

or

$$K \le 0.141\,\sigma_{ys}\sqrt{\pi a}$$

Therefore for a centre cracked plate, the applied stress has to be less than approximately 14.1% of the yield stress of the material; otherwise the stress intensity factor K would no longer provide a unique characterising parameter. Under plane strain condition, however, the applied stress can be higher, up to 35%. This will be discussed later.

3.2 The Strip Yield Model

A different approach to finding the extent of the plastic zone was proposed by Dugdale and Barenblatt, who considered a long, slender plastic zone at the crack tip in a non-hardening material in plane stress. The strip yield plastic zone is modelled by assuming a crack of length $2a + 2\rho$ where ρ is the length of the plastic zone, with a closure stress equal to σ_{ys} applied at each crack tip, see Fig.3.2. The size of ρ is chosen such that the stress singularity vanishes at the end of the effective crack:

$$K_\sigma + K_\rho = 0 \tag{3.7}$$

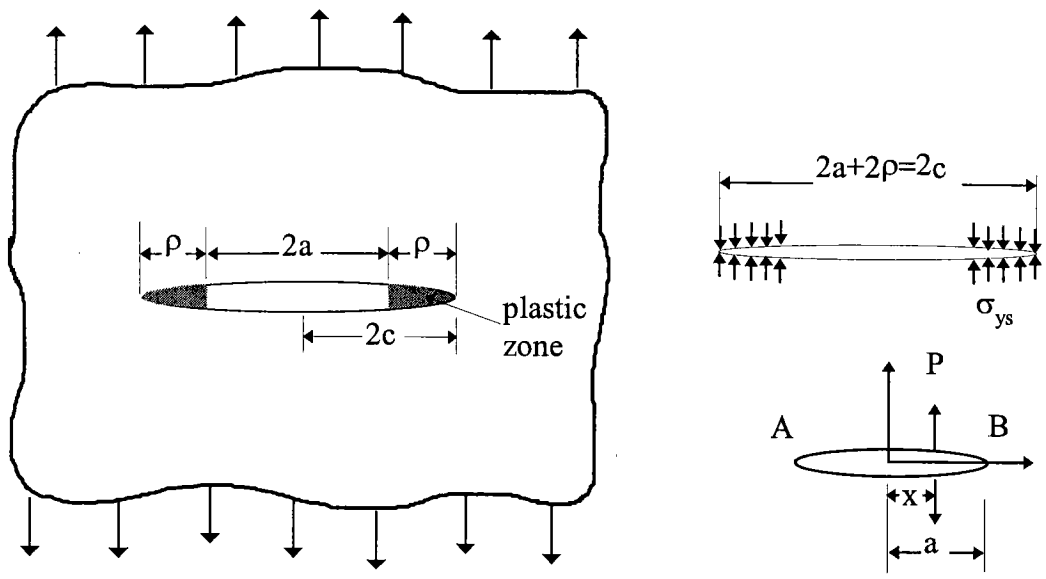

Fig.3.2 The strip yield approach.

The stress intensity due to the closure stress can be estimated by considering a normal force P applied to the crack at a distance x from the centre line of the crack; the resultant stress intensity factors at the two crack tips are,

$$K_A = \frac{P}{\sqrt{\pi a}}\sqrt{\frac{a+x}{a-x}} \tag{3.8}$$

$$K_B = \frac{P}{\sqrt{\pi a}}\sqrt{\frac{a-x}{a+x}} \tag{3.9}$$

Here the closure force at a point within the strip yield zone is

$$P = -\sigma_{ys}dx \tag{3.10}$$

thus the total stress intensity at each crack tip resulting from the closure stresses is obtained by replacing a with $a+\rho=c$ and so

$$\begin{aligned} K_\rho &= -\frac{\sigma_{ys}}{\sqrt{\pi c}}\int_a^c\left\{\sqrt{\frac{c-x}{c+x}}+\sqrt{\frac{c+x}{c-x}}\right\}dx \\ &= -\frac{2\sigma_{ys}c}{\sqrt{\pi}}\int_a^c\frac{dx}{\sqrt{c^2-x^2}} = -\frac{2}{\pi}\sigma_{ys}\sqrt{\pi c}\cos^{-1}\left(\frac{a}{c}\right) \end{aligned} \tag{3.11}$$

The stress intensity from the remote tensile stress, $K_\sigma = \sigma\sqrt{\pi c}$, thereafter, equation (3.7) leads to

$$\frac{a}{c} = \cos\left(\frac{\pi}{2}\frac{\sigma}{\sigma_{ys}}\right) \tag{3.12a}$$

i.e.

$$\rho = a\left(\sec\left(\frac{\pi}{2}\frac{\sigma}{\sigma_{ys}}\right) - 1\right) \tag{3.12b}$$

Neglecting the higher order terms in the series development of the cosine, ρ is found

$$\rho = \frac{\pi K^2}{8\sigma_{ys}^2} \qquad (\frac{\sigma}{\sigma_{ys}} << 1.0) \tag{3.13}$$

which is of the same order as equation (3.4) (the difference is about 23%).

3.3 Plane Stress versus Plane Strain.

From Chapter 2, the triaxial stress state directly ahead of a crack tip is, $\sigma_1 = \sigma_2 = \sigma_{yy}$, σ_3=0 for plane stress and $\sigma_3 = 2\nu\sigma_{yy}$ for plane strain. According to the Von Mises yield criterion, in terms of principal stresses,

$$(\sigma_1 - \sigma_2)^2 + (\sigma_2 - \sigma_3)^2 + (\sigma_3 - \sigma_1)^2 = 2\sigma_{ys}^2 \tag{3.14}$$

where σ_{ys} is the uniaxial yield stress. It can be easily shown that

$$\sigma_y = \begin{cases} \dfrac{\sigma_{ys}}{1-2\nu} & \text{plane strain} \\ \sigma_{ys} & \text{plane stress} \end{cases} \tag{3.15}$$

For ν=1/3 we have effective yield stress $\sigma_y = 3\sigma_{ys}$ for plane strain. This means the plastic zone size under plane strain condition is approximately one ninth that under plane stress condition. In general, the effective yield stress can be expressed as,

$$\sigma_y = \alpha\sigma_{ys} \tag{3.16}$$

where α is termed the plasticity constraint factor. From previous analysis, α=1 for plane stress and α=3 for plane strain. For a finite thickness plate, an empirical value often used is $\alpha = \sqrt{3}$, that is,

$$\alpha = \begin{cases} 1.0 & \text{plane stress} \\ 1.732 & \text{finite thickness} \\ 3.0 & \text{plane strain} \end{cases} \tag{3.17}$$

Therefore the size of the plastic zone under plane strain condition is smaller than under plane stress condition by a factor of 1.732. In this case, the maximum applied stress level above which LEFM would become invalid is approximately three times higher, up to 35%.

Example 3.10 Determine the plastic zone length at fracture for a mild steel with K_{Ic} = 70 MPa$\sqrt{m}$ and σ_{ys} = 450 MPa for (a) plane stress and (b) finite thickness condition.

Solution Under plane stress condition,

$$r_p = \frac{1}{\pi}\left(\frac{K_{IC}}{\sigma_{ys}}\right)^2 = \frac{1}{3.14}\left(\frac{70}{450}\right)^2 = 7.7\times10^{-3} \quad \text{(m)}$$

and for finite thickness condition (taking $\alpha = \sqrt{3}$),

$$r_p = \frac{1}{\pi}\left(\frac{K_{IC}}{\sqrt{3}\sigma_{ys}}\right)^2 = \frac{1}{3.14}\left(\frac{70}{\sqrt{3}\times450}\right)^2 = 2.567\times10^{-3} \quad \text{(m)}$$

3.4 Shapes of Plastic Zone

As the stress state ahead of a crack tip is three-dimensional, the shape of the plastic zone is not necessarily a circle, but needs to be determined using an appropriate yield criterion. Either the Tresca criterion or the Von Mises criterion is usually applied. Adopt the von Mises criterion given by equation (3.12), noting the crack tip stress distributions given by equations (2.29) and (2.30), the boundary of the plastic zone as a function of θ can be derived for plane stress condition and plane strain condition $[\sigma_3 = \nu(\sigma_1 + \sigma_2)]$, respectively,

$$r_1(\theta) = \frac{K^2}{4\pi\sigma_y^2}\left[1 + \frac{3}{2}\sin^2\theta + \cos\theta\right] \quad \text{plane stress} \tag{3.18}$$

$$r_1(\theta) = \frac{K^2}{4\pi\sigma_y^2}\left[\frac{3}{2}\sin^2\theta + (1-2\nu)^2(1+\cos\theta)\right] \quad \text{plane strain} \tag{3.19}$$

These two equations are plotted in Fig.3.3. Note that these are the first order estimates. Nevertheless, it indicates significant differences in the sizes and shapes of the mode I plastic zones for plane stress and plane strain conditions. The latter condition suppresses yielding, resulting in a smaller plastic zone for a given stress intensity factor. Similar equations can also be obtained for Mode II and Mode III.

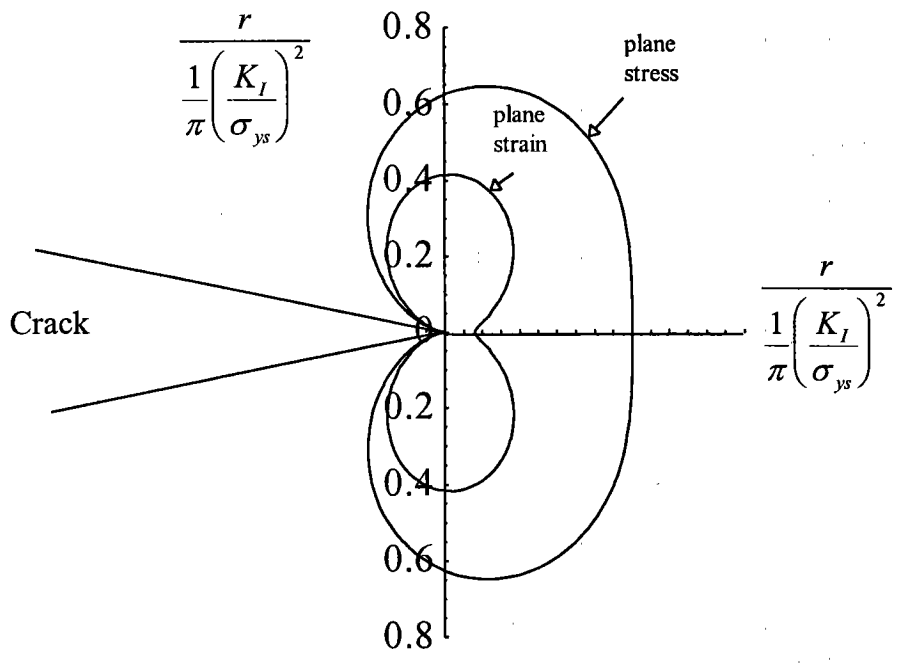

Fig.3.3 Crack tip plastic zone shapes under mode I loading

A modification similar to that outlined in section 3.1 can also be carried out to improve the above estimate; the second order estimate is just twice that given in equations (3.18) and (3.19), i.e.

$$r_p(\theta) = 2r_1(\theta) \tag{3.20}$$

The three dimensional slip planes of a mode I crack are shown in Fig.3.4 for plane stress and plane strain. For a finite plate, due the free surface effect, the plastic zone looks like a 'dog-bone', as depicted in Fig.3.4. Due to this thickness effect, the plastic constraint factor normally lies between 1 and 3, for example α=1.7. It is important to point out that although the plastic zone at the middle of the plate is smaller than that near the surface, the high triaxial stress that exists at the middle of the plate (this is sometimes called plastic constraint) causes crack growth to occur there first, under both static and fatigue conditions.

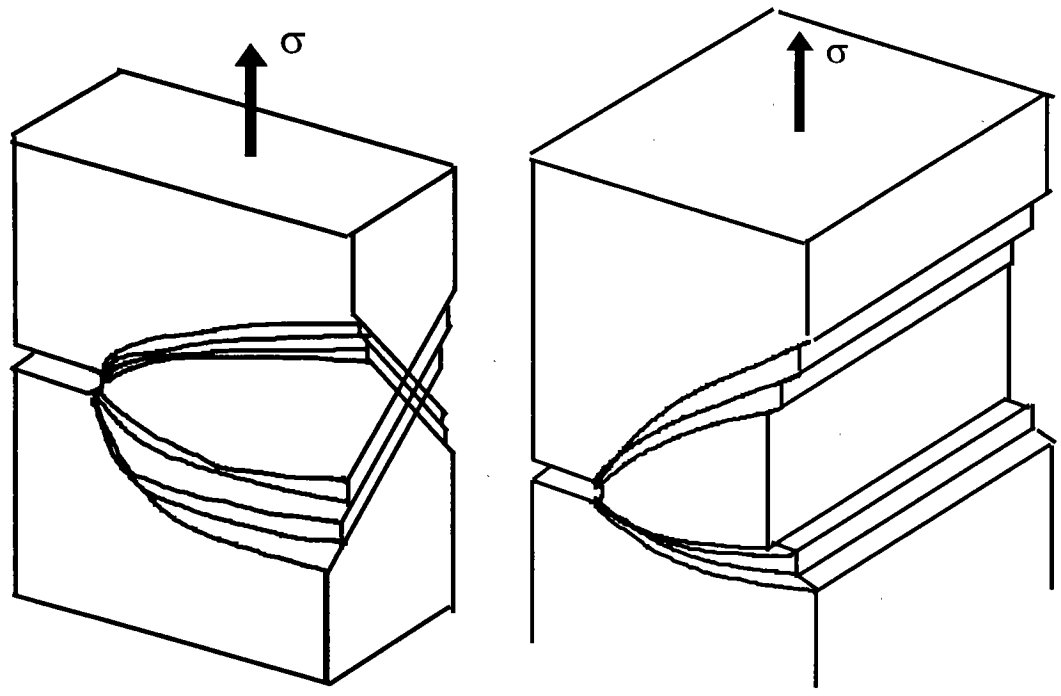

Fig.3.4 Slip-planes around a mode I crack for (a) plane stress and (b) plane strain

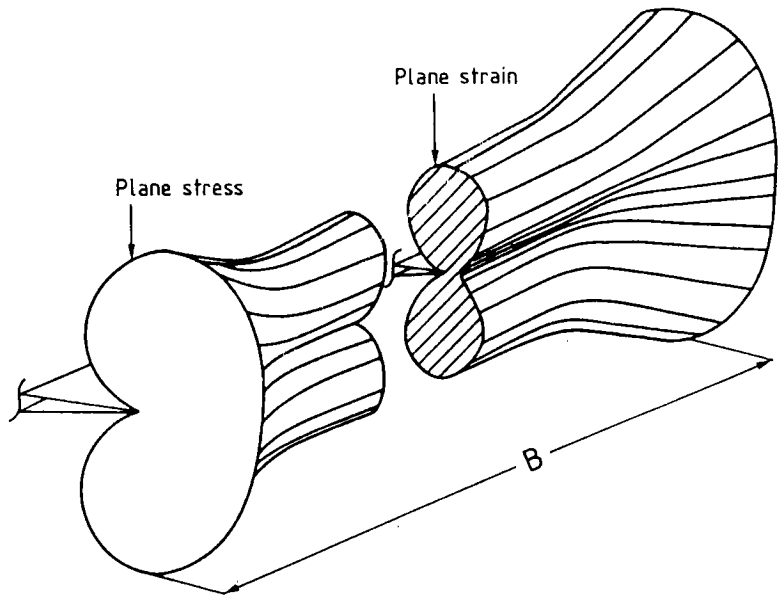

Fig.3.5 Schematic representation of the three-dimensional nature of the plastic zone around a crack tip in finite plate

3.5 Crack Tip Opening Displacement

Due to plastic deformation at crack tip, the originally point sharp crack tip would become blunt (otherwise stress singularity will exist), resulting in a finite radius at the tip of the initial crack. This phenomenon is normally called crack tip opening, as if the tip of the crack opens up. One simple way of estimating this radius is through the fictitious crack method discussed in section 3.1. Since the fictitious crack tip is at a distance $r_p/2$ ahead of the initial crack tip, a finite gap now exists between the faces of the fictitious crack at the tip of the initial crack, as depicted in Fig.3.6, which is equal to

$$\delta = 2u_y = \frac{4K_I}{E'}\sqrt{\frac{(a+r_p/2)^2 - a^2}{\pi a}} = \frac{4K_I}{E'\pi}\left(\frac{K_I}{\sigma_y}\right) = \frac{4K_I^2}{\pi E'\sigma_y} \tag{3.21}$$

where E' and σ_y are the effective Young's modulus and yield stress, respectively, which are defined by equations (1.8) and (3.16) for plane stress and plane strain. This is shown in Fig.3.7.

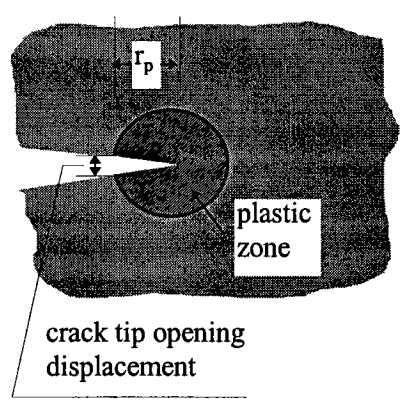

Fig.3.6 Crack tip opening displacement.

A similar estimate can be obtained from the strip yield model, although the calculations are slightly more involved. Here only the final result is given,

$$\delta = \frac{8\sigma_y a}{\pi E'}\ln\left(\sec\left(\frac{\pi\sigma}{2\sigma_y}\right)\right) \approx \frac{K_I^2}{E'\sigma_y} \tag{3.22}$$

which is about 27 per cent lower than the Irwin model prediction. Again E' and σ_y for plane strain condition are as defined previously. The fact that the crack tip would attain a finite radius due to plastic deformation makes the distinction between notch and crack even more blurry. But it is important to note that the crack tip opening displacement is stress dependent, unlike notch root radius.

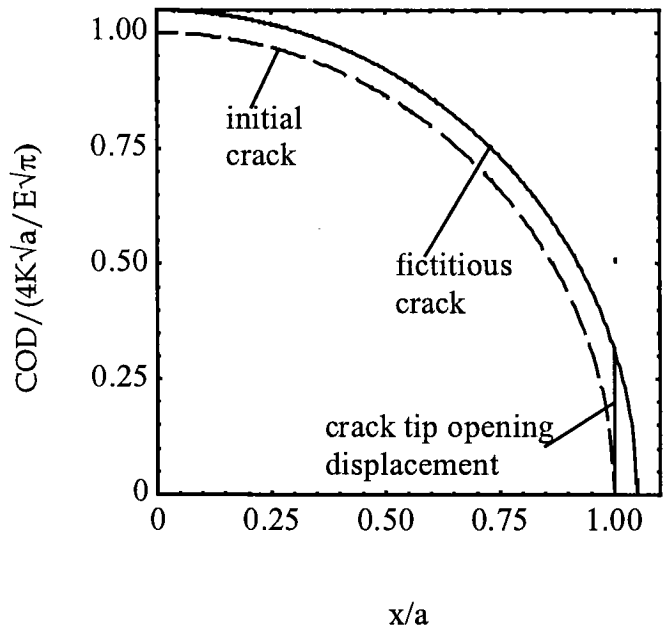

Fig.3.7 Opening profile of a fictitious crack

However, the definition of crack tip opening displacement in general is not so straightforward, as the relative displacement between the upper and lower crack faces at the very tip of the crack is mathematically zero. A more general, alternative definition is given by Rice (1968): crack tip opening displacement is defined as the opening where 45^0 lines emanating back from the crack tip intercept the crack faces, as depicted in Fig.3.8. Often the crack opening profile behind the crack tip is plotted versus the distance from the crack tip, and then the height at the intersection between the crack opening curve and line $u_y = r$ is defined as the crack tip opening displacement.

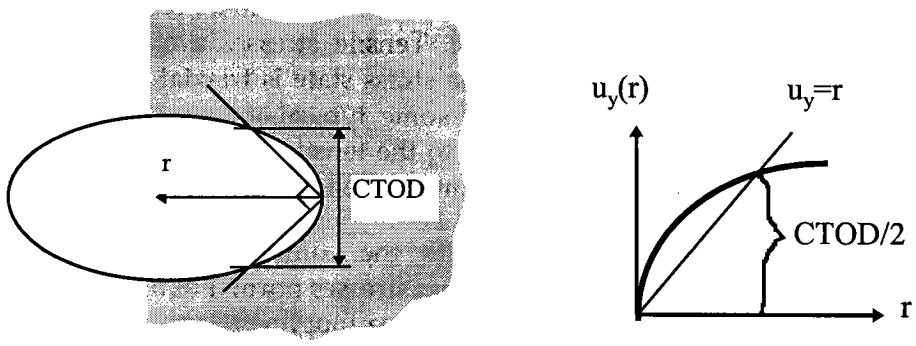

Fig.3.8 Definition of CTOD and possible Finite Element Method procedure

4. Fracture Criteria

4.1 K as a Failure Criterion

From previous analysis, it is clear that when stresses at the crack tip exceed yield (which always happens for engineering materials), plasticity results. However, if the redistribution of stress has a minimal effect on the crack tip elastic stress field, then the K approach to defining the stress field is still of sufficient accuracy for engineering applications. Thus, if plasticity is minimal, then a LEFM approach is justified.

Of importance to practical applications is the critical stress and strain state at the crack tip zone, which, when attained, causes the crack to propagate in a brittle, catastrophic manner. The most dangerous situation occurs when a crack is in a high-energy but constrained field that permits only slight plastic deformation at the crack tip. Expressed another way, the amount of energy absorbed in plastic deformation is reduced to a minimum extent and much more energy is thus available for fracture, i.e. crack propagation. This critical state can be described by a critical stress intensity factor K_c,

$$K = K_C \tag{4.1}$$

which may imply either a low stress acting on long crack or a small crack suffering a high stress. It is important to note the different meaning of the two sides of the above equation. The left hand side represents the driving force of the crack, which depends on the applied loads and the geometry of the components. The right hand side of equation (4.1) signifies the materials' resistance to fracture, which is an environment and load rate dependent material property.

Laboratory testing indicates that the fracture toughness value depends on the thickness B of the specimen tested. The plane strain fracture toughness of the materials is a material property (denoted as K_{IC}, where subscript I denotes mode I loading). Under plane strain condition, since the crack tip plastic zone is small in relation to the component thickness, plastic contraction in the through thickness direction is suppressed by the surrounding elastic material. Tensile stresses are set up in the thickness direction of the plastic zone so that the stress state is triaxial, giving rise to constrained plastic deformation. Table 4.1 lists some typical values of plane strain fracture toughness. As before, the suffix I refers to the tensile opening mode of crack extension, whilst II and III symbolise shear and anti-plane tear modes, respectively.

When the plastic zone is large compared with the component's thickness, the triaxiality may be relaxed and the through thickness stresses normal to the plane of the component will be negligible. In this case, the fracture toughness may vary with the specimen thickness, B. The form of variation of Kc with specimen thickness is schematically shown in Fig. 4.1. Beyond a certain thickness, a state of plane strain prevails (see Chapter 3) and the toughness reaches asymptotic value. If the thickness of the specimen is reduced, more energy will be dissipated as a result of plastic deformation near the specimen surface which is under plane stress condition. There

seems to exist an optimum thickness where the toughness reaches its highest level, see Fig.4.1.

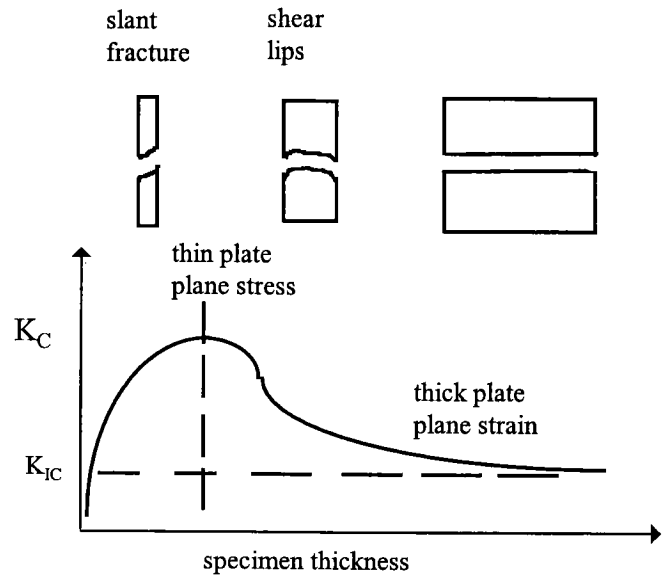

Fig.4.1 Effect of thickness on fracture toughness

In order to achieve plane strain conditions at the elastic-plastic interface, the plastic zone must be small compared to the specimen thickness, crack length, and width of ligament:

$$r_p \le \frac{a}{50}, \quad \frac{W}{50}, \quad \frac{B}{50} \tag{4.2}$$

According to the ASTM standard, the following requirements must be satisfied

$$a, B, (W-a) \ge 2.5\left(\frac{K_I}{\sigma_{ys}}\right)^2 \tag{4.3}$$

which is equivalent to setting the plasticity constraint factor to be $\sqrt{3}$.

Table 4.1 Typical values of fracture toughness

Material	Young's modulus E (GPa)	Yield stress σ_{ys} (MPa)	Toughness K_{IC} (MPa$\sqrt{m}$)	Thickness requirement 2.5 $(K_{IC}/\sigma_{ys})^2$ (mm)
Steels	210			
medium carbon		260	54	108
pressure vessel		470	208	489.6
high strength alloy		1460	98	11
AFC 77 stainless		1530	83	7.4
Aluminium alloys	72			
2024 T8		420	27	10.4
7075 T6		540	30	7.9
7178 T6		560	23	4.2
Titanium alloys	108			
Ti-6Al-4V		1060	73	12.6
(high yield)		1100	38	3.1
Comparative data				
Concrete	45	80	0.2-1.4	
Ice	9.1	85	0.2*	
Epoxy	2-3	30-60	0.5-3	
Boron fibre	441	3000		
Carbon fibre	250-390	2200-2700		
Boron/epoxy composite	220-340	725-1730	46	
CFRP	70-200	300-1400	32-45	
GFRP	38	100-300	20-60	

- **not at room temperature !**

4.2 Residual Strength and Critical Crack Size

Since the severity of a cracked component is characterised by stress intensity factor, K, and failure will occur when $K = Kc$, the residual strength of a cracked component is,

$$\sigma_c = \frac{K_C}{Y\sqrt{\pi a}} \tag{4.4}$$

where Y is a geometry correction factor. Note that the stress σ is the gross stress on the section on which the function a is defined, where residual strength implies a net section condition. In the case of plane strain $K_c = K_{IC}$. It is conservative to assume that $K_c = K_{IC}$ if the detailed stress state is not known. The size of the crack at this stress is called the 'critical crack size'. This is normally difficult to solve in closed form as $Y(a)$ is normally a complicated function of crack length and component geometry. Nevertheless, it can be solved numerically through iteration or, if the value of Y varies slowly with crack size, e.g. for a relatively small crack in a wide panel, an approximate value may be used. The critical crack size that a component can tolerate for a given load is

$$a_c = \frac{1}{\pi}\left(\frac{K_C}{Y(a_c / W)\sigma}\right)^2 \tag{4.5}$$

The above two equations provide the basis for fracture mechanics based design methodologies.

It should be pointed that equation (4.4) is valid only when linear fracture mechanics is applicable, that is the net section stress level is far below the material's yield stress. Otherwise the component will fail in a different mode: plastic collapse. Consider a centre cracked panel with a finite width W, the absolute highest load carrying capability is bounded by the plastic collapse strength: the stress level over the entire section exceeds the yield or ultimate tensile strength of the material. It is easy to show that the nominal stress at collapse is

$$\sigma_{pc} = \frac{W - 2a}{W}\sigma_{ys} \tag{4.6}$$

When this happens, the plastic deformation becomes unbounded and fracture will occur, regardless of the fracture toughness.

Therefore there are two possible failure modes: brittle fracture and plastic collapse. Should the fracture stress σ_c be higher than the stress causing failure by collapse, then collapse will prevail. As a result, the actual residual strength is the lowest of σ_c and σ_{pc}. Considering a centre cracked panel, there are three situations in which a plastic collapse failure would prevail: (1) the toughness is very high; (2) the crack is very small; and (3) the width W is very small. A sketch is shown in Fig.4.2. The intersection of the two curves is given by

$$\frac{W - 2a}{W}\sigma_{ys} > \frac{K_c}{\sqrt{\pi a}\sqrt{\sec(\pi a / W)}} \tag{4.7}$$

In the short crack regime, the exact transition from one mechanism to the other is not clear, but a plausible engineering approximation is the 'tangent' rule: drawing a tangent line passing through the ultimate tensile strength point. More accurate prediction can be achieved by using elasto-plastic fracture mechanics methods.

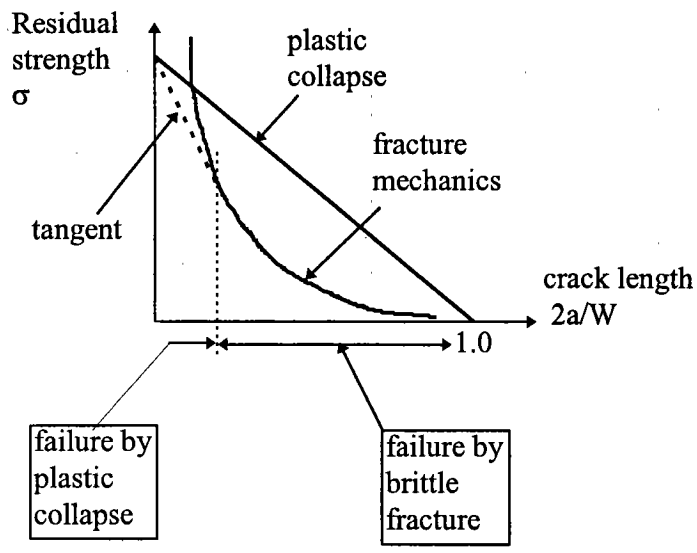

Fig.4.2 Competition between fracture and collapse

Example 4.11 Estimate the failure load under uniaxial tension for a centre-cracked panel of aluminium alloy of width W=500 mm, and thickness B=4 mm, for the following values of crack length $2a$ = 20 mm and $2a$ = 100 mm. Yield stress σ_y=350 MPa and fracture toughness K_{Ic}=70 MPa$\sqrt{m}$

Solution There are two possible failure modes: plastic collapse and brittle fracture. We will assess the load level required for each mode to prevail.

(i) $2a$ = 20 mm.

Plastic collapse load $F_{pc} = \sigma_{ys} \cdot (W - 2a) \cdot B = 672$ kN

Fracture load $F_c = \sigma_c \cdot W \cdot B$ where $\sigma_c = \dfrac{K_{IC}}{\sqrt{\pi a \sec(\pi a / W)}} = 394.6$ MPa

thus F_c = 790 kN.

The actual failure load is the smaller of the above results, 672 kN.

(ii) $2a$ = 100 mm.

Plastic collapse load $F_{pc} = \sigma_{ys} \cdot (W - 2a) \cdot B = 560$ kN

Fracture load $F_c = \sigma_c \cdot W \cdot B$ where $\sigma_c = \dfrac{K_{IC}}{\sqrt{\pi a \sec(\pi a / W)}} = 172.2$ MPa

thus F_c = 334.57 kN.

The actual failure load is the smaller of the above results, 334.6 kN.

4.3 *R*-curve

Crack extension occurs when the stress intensity factor or the strain energy release rate attains a critical value. In a truly brittle material like glass or ice, the energy for crack growth is the surface energy to form the new surface, i.e

$$G = 2\gamma_f \tag{4.8}$$

where the factor "2" is included to represent the two crack surfaces being created. It should be noted that the energy required for a crack to grow in an engineering material is much larger than the surface energy. This is because plastic deformation will inevitably occur near the crack tip region and during crack extension energy is consumed in deforming the material plastically. In general the fracture criterion can be written as

$$G = 2W_f = 2(\gamma_f + \gamma_p) \tag{4. 9}$$

Where γ_p refers the plastic work per unit area of surface created, and is typically much larger than γ_f.

Normally it is convenient to replace $2W_f$ with R, the material resistance to crack extension. A plot of R versus crack extension is called a resistance curve or R curve, whereas the plot of G versus crack extension is the driving force curve. It is important to note that the driving force curve is entirely dependent on the structure geometry and loading condition, whilst the R curve is a material property dependent on temperature, environment, and loading rate etc. Most brittle materials exhibit a constant resistance sometimes called "no R-curve" effect, as shown in Fig.4.3(a). Many ductile materials, such as low strength steels, possess a rising R curve : a plastic zone at the tip of crack increases with crack length, hence the energy that would dissipate to overcome plastic deformation would increase. This is illustrated in Fig.4.3(b). The exact shape of the R curve depends on the material and, to a lesser extent, on the configuration of the cracked structure.

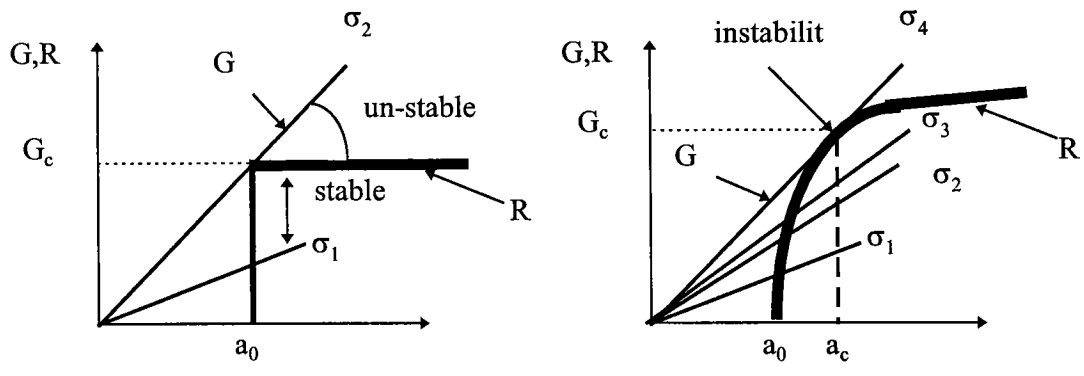

Fig 4.3. Schematic driving force and R curve diagrams

If a component, containing a crack or crack-like defect, and experiencing some plasticity in the vicinity of the crack, is loaded by increments the crack will extend and stop after each increase in load. This condition is defined as slow-stable crack growth. In this condition the value of the material resistance K_R is equal to the applied value K at any given applied stress. Consequently the fracture toughness (Kc) may be obtained by the use of crack growth resistance curves (commonly called R-curves). These curves are a continuous record of toughness development in terms of crack growth resistance, denoted K_R, plotted against crack extension under continuously increasing values of stress intensity factor, K. The R-curves characterise the resistance to fracture of materials during incremental slow-stable crack extension as a result of the growth of the plastic zone as the crack extends.

Consider a plate with a through crack of initial length $2a_0$. At a fixed remote stress, σ, the energy release rate varies linearly with crack size. If the material has a flat R-curve, as shown in Fig 4.3(a), one can define a critical value of energy release rate, G_C, unambiguously. The crack will grow if the applied G reaches this value. For materials with a rising R curve, such as a crack plate reinforced with a composite patch, however, one cannot uniquely characterise a single value toughness value. In this case, normally we define that crack growth will occur when

$$\frac{dG}{da} > \frac{dR}{da} \text{ and } G \geq R \qquad (4.10)$$

This corresponds to when the driving force curve is tangent with the R curve, as depicted in Fig.4.3(b). This can be interpreted as the critical condition when the energy available in the component for crack growth exceeds the maximum amount that the material can dissipate. This point of tangency depends on the shape of the driving force, which itself depends on the shape of the configuration of the structure. For example, the driving force curve for a through crack configuration is linear, but G in the double cantilever beam specimen varies with a^2; these two configurations would have different G_C values for a given R curve.

Example 4.12 The following data were obtained from a series of tests conducted on pre-cracked specimens of thickness 10 mm,

Crack length	Critical load	Critical displacement
a (mm)	P (kN)	u (mm)
30	4	0.4
40	3.5	0.5
50.5	3.12	0.63
61.6	2.8	0.78
71.7	2.67	0.94
79	2.56	1.09

where P and u are the critical load and displacement at each crack growth. The load displacement record for all crack lengths is linear up to a critical point. Determine the

critical value of the strain energy release rate Gc=R from (a) the load displacement records and (b) the compliance-crack length curve.

Solution The load-deflection curve can be constructed from the tabulated data, as shown in Fig.4.4(a). The area for a triangle depicted in Fig.4.4(b) is,

$$\text{Area} = P_1 u_2 - \frac{1}{2} P_1 u_1 - \frac{1}{2} P_2 u_2 - \frac{1}{2}(P_1 - P_2)(u_2 - u_1) = \frac{1}{2}(P_1 u_2 - P_2 u_1)$$

and so the energy released during each crack growth can be calculated

$$G = R = \frac{\text{Area}}{2\Delta a \cdot B} = \frac{\frac{1}{2}(P_i u_j - P_j u_i)}{2B(a_j - a_i)}$$

The results for the five crack increments are: 30.0, 30.7, 30.2, 29.1, 30.8. (The unit is kJ/m^2). Clearly this material exhibits little R-curve behaviour.

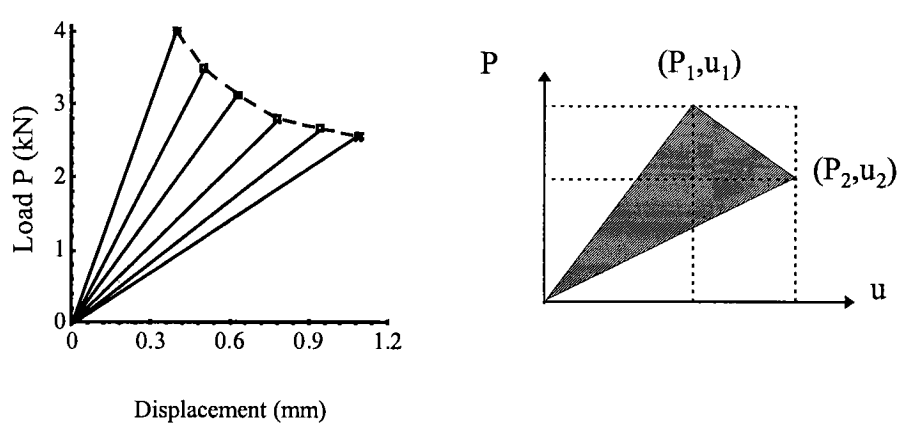

Fig.4.4 Load-deflection curve

4.4 Mixed Mode Loading: Fracture and Crack Path

Most structures and components are subjected to more than one loading. When two or more modes of loading are present, equation (2.20) indicates that energy release rate contributions from each mode are additive. This equation assumes self-similar crack growth, however. If we consider an angled crack problem as depicted in Fig.4.5, coplanar growth means that the crack would grow at an angle $90^0 - \beta$ degrees from the applied stress. In practice, the crack tends to propagate in a direction orthogonal to the applied normal stress; i.e. the mixed-mode crack becomes a mode I crack. This is because a propagating crack seeks the path of least resistance (or the path of maximum driving force, or the path that the maximum amount of energy can be released) and need not be confined to its initial plane. A number of criteria have been proposed to account for such effects. Among them, the most widely used are (i) crack growth will

take place in the direction of maximum energy release rate; (ii) crack growth occurs in a direction perpendicular to the maximum principal stress; (iii) crack growth occurs where the strain energy density is the minimum. It can be shown that criteria (i) and (ii) are identical and the differences between these criteria are generally small.

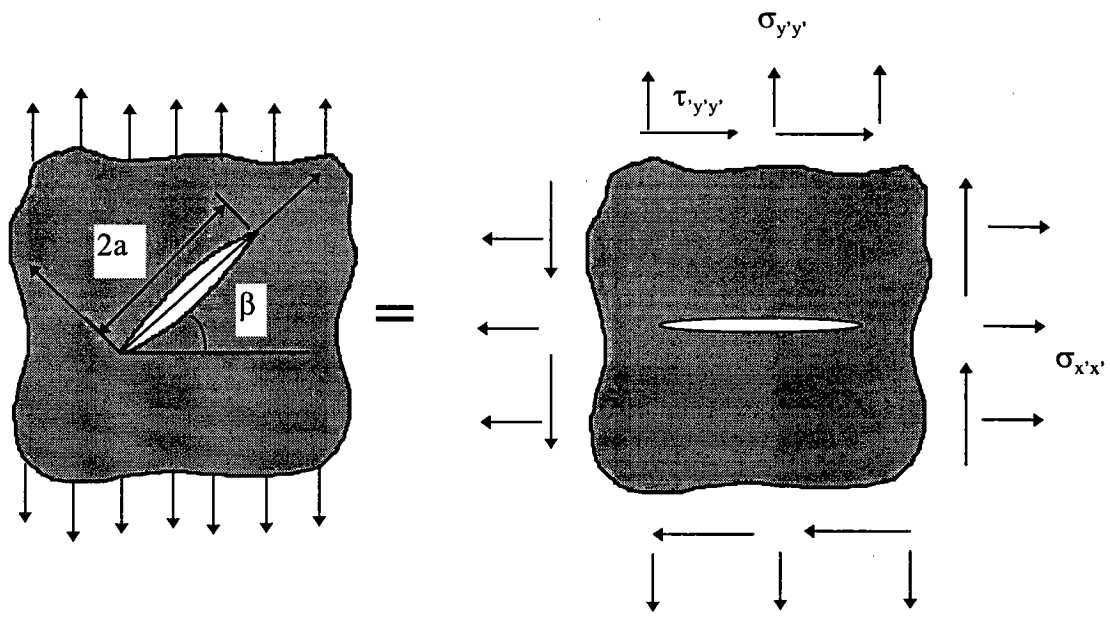

Fig. 4.5 Through crack in an infinite plate under mixed mode loading

If a crack is loaded in combined mode I and II, the stresses σ_θ and $\tau_{r\theta}$ at the crack tip can be derived from the expressions in Table.2.2, by adding the stresses due to the separate mode I and mode II. The result is as follows:

$$\sigma_\theta = \frac{1}{\sqrt{2\pi r}}\cos^2\left(\frac{\theta}{2}\right)\left[K_I\cos\frac{\theta}{2} - 3K_{II}\sin\frac{\theta}{2}\right] \qquad (4.11)$$

$$\tau_{r\theta} = \frac{1}{\sqrt{2\pi r}}\cos\frac{\theta}{2}\left[K_I\sin\frac{\theta}{2}\cos\frac{\theta}{2} + K_{II}(1-3\sin^2\frac{\theta}{2})\right] \qquad (4.12)$$

Suppose that the crack in question forms an infinitesimal kink at an angle α from the plane of crack, as shown in Fig.4.6. The local stress intensity factors at the tip of this kink differ from the nominal K values of the main crack. If we define a local $x'-y'$ coordinate system at the tip of the kink, we can define the local mode I and mode II stress intensity factors,

$$K_I(\alpha) = \lim_{r\to 0}\sigma_\theta\sqrt{2\pi r} = \cos^2\frac{\alpha}{2}\left[K_I\cos\frac{\alpha}{2} - 3K_{II}\sin\frac{\alpha}{2}\right] \qquad (4.13)$$

$$K_{II}(\alpha) = \lim_{r\to 0}\tau_{r\theta}\sqrt{2\pi r} = \cos\frac{\alpha}{2}\left[K_I\sin\frac{\alpha}{2}\cos\frac{\alpha}{2} + K_{II}(1-3\sin^2\frac{\alpha}{2})\right] \qquad (4.14)$$

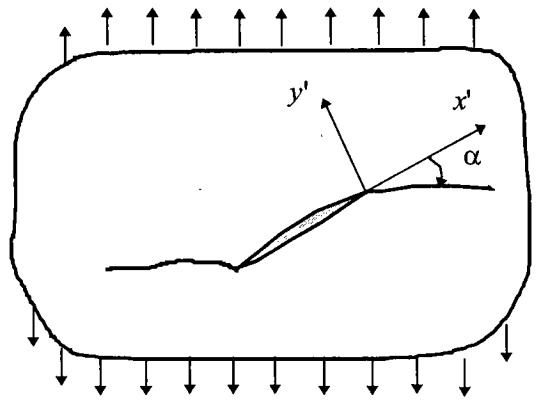

Fig.4.6 Kink at the tip of a crack inclined at an angle to the applied load

The energy release rate for the kinked crack is

$$G(\alpha) = \frac{K_I^2(\alpha) + K_{II}^2(\alpha)}{E} \tag{4. 15}$$

According to the energy release rate criterion, crack propagation would occur in a direction along which the above energy release rate attains a maximum value. This is shown in Fig. 4.7, where the energy release rate $G(\alpha)$ is normalised by $G(\alpha = 0)$.

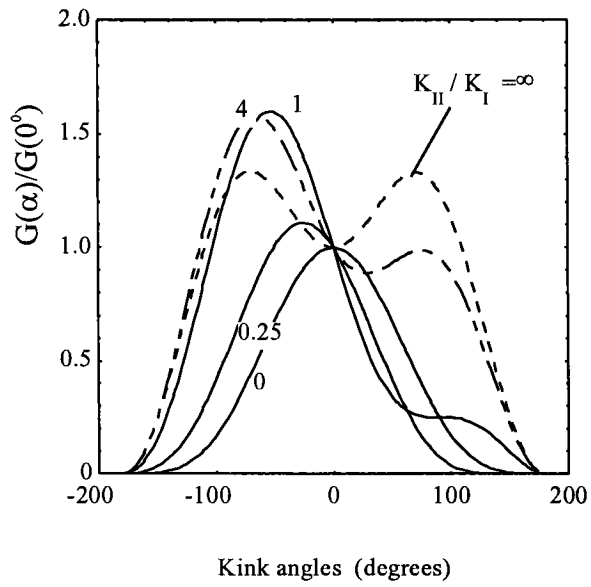

Fig.4.7 Local energy release rate at the tip of a kinked crack

Since

$$\frac{dK_I}{d\alpha} = -\frac{3}{2}K_I \cos^2\frac{\alpha}{2}\sin\frac{\alpha}{2} - \frac{3}{2}K_{II}\cos\frac{\alpha}{2}\left(1-3\sin^2\frac{\alpha}{2}\right) \equiv -\frac{3}{2}K_{II}$$

the maximum of the strain energy release rate $dG(\alpha)/d\alpha = 0$ is equivalent to $K_{II}(\alpha) = 0$ or $dK_I/d\alpha = 0$, thus the peak in $G(\alpha)$ at each α_0 corresponds to the point where $K_I(\alpha)$ exhibits a maximum and $K_{II}(\alpha_0)$=0. In other words, the energy release rate criterion is identical to maximum hoop stress criterion. Figs.4.8 show the hoop stress distributions for three mixed mode ratios: $K_{II}/K_I = 0$ (mode I), $K_{II}/K_I = 1$, $K_{II}/K_I = \infty$ (mode II).

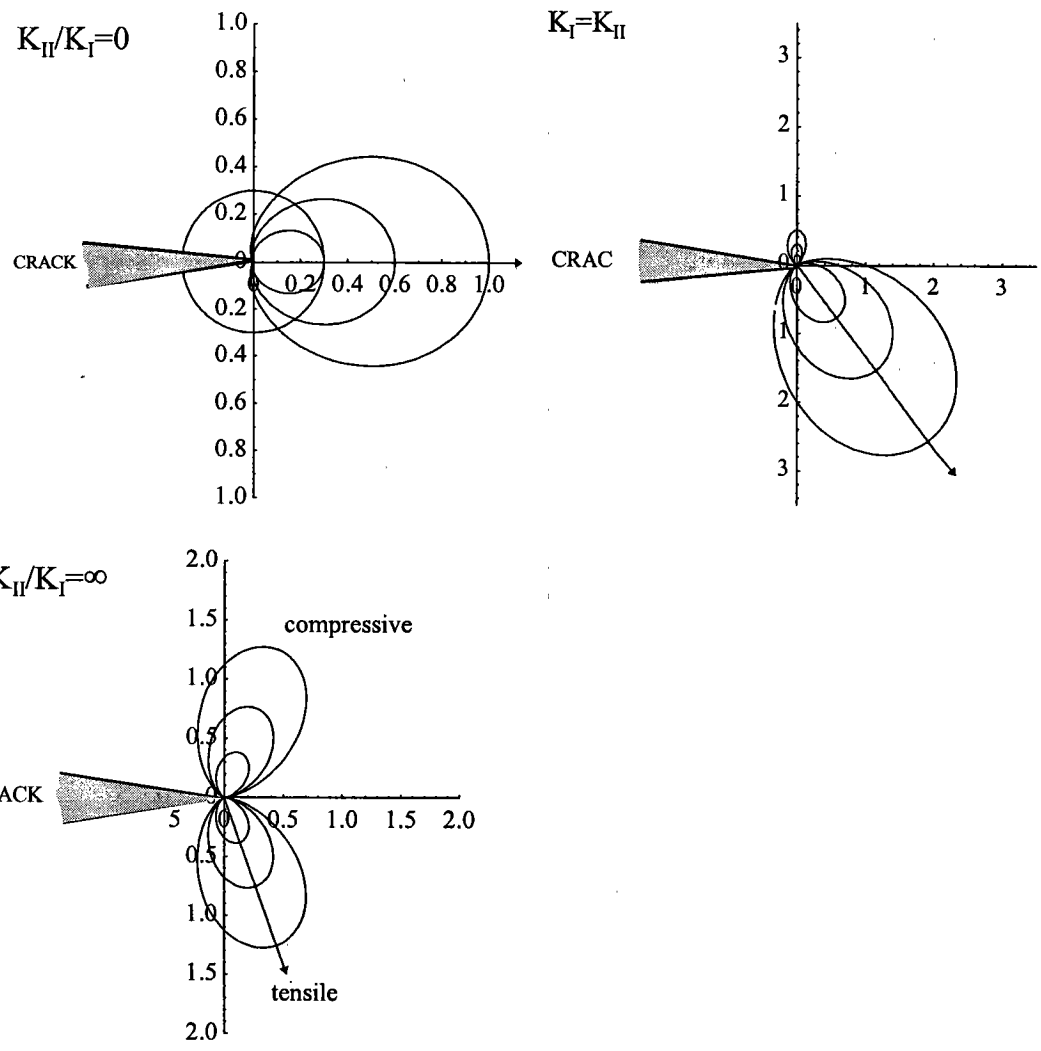

Fig.4.8 Distributions of hoop stress for various mixed mode ratios

The arrows in the figures mark the direction of crack propagation, which is given by the following equation

$$K_{II}(\alpha_0)=0 \tag{4.16}$$

so

$$K_I \sin\frac{\alpha_0}{2}\cos\frac{\alpha_0}{2}+K_{II}(1-3\sin^2\frac{\alpha_0}{2})=0 \tag{4.17}$$

which yields,

$$\left(\tan\frac{\alpha_0}{2}\right)_{1,2}=\frac{1}{4}\frac{K_I}{K_{II}}\pm\sqrt{\left(\frac{K_I}{4K_{II}}\right)^2+\frac{1}{2}} \tag{4.18}$$

The critical value of K_I or K_{II} at which crack propagation occurs can be determined from the following equation,

$$K_I(\alpha)=K_{IC} \quad \text{i.e.} \quad K_I\cos^3\frac{\alpha_0}{2}-3K_{II}\cos^2\frac{\alpha_0}{2}\sin\frac{\alpha_0}{2}=K_{IC} \tag{4.19}$$

Example 4.13 Determine the propagation angle for an inclined crack subjected to uniaxial tension.

Solution: Assume the crack is inclined at an angle β to the applied load, as depicted in Fig.4.5. The mode I and mode II stress intensity factors can be determined as,

$$K_I=\sigma\sqrt{\pi a}\cos^2\beta \qquad \text{and} \qquad K_{II}=\sigma\sqrt{\pi a}\cos\beta\sin\beta$$

consequently the mode I to mode II ratio is equal to $(1/\tan\beta)$, hence the kink angle is equal to $\beta+\alpha_0$,

$$\beta+\alpha_0=\beta+2\tan^{-1}\left(\frac{1}{4\tan\beta}-\sqrt{\left(\frac{1}{4\tan\beta}\right)^2+\frac{1}{2}}\right)$$

which is depicted in Fig.4.9, together with some experimental data.

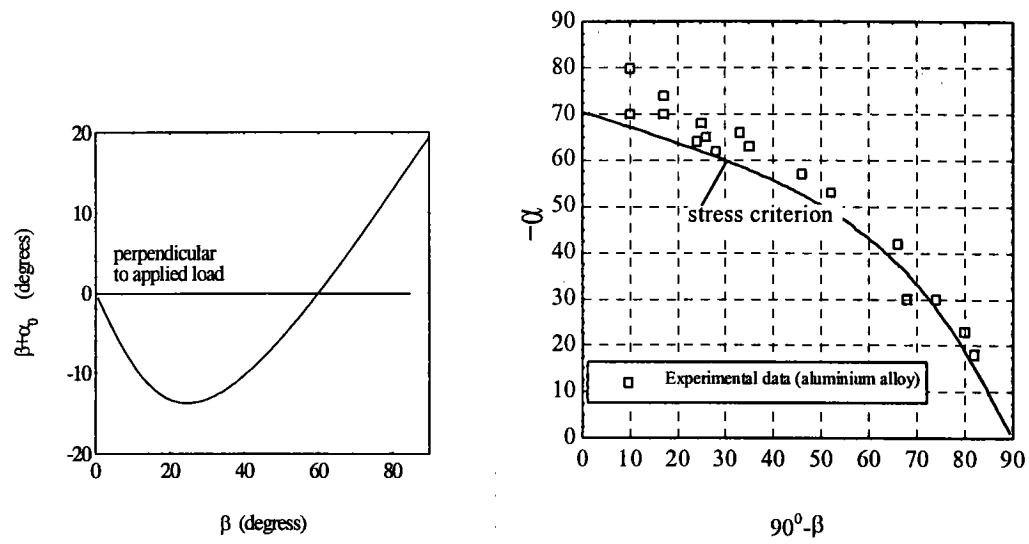

Fig.4.9 Variation of crack extension angle versus the crack inclination angle β.

5. Fatigue and Life Prediction

5.1 Fatigue Crack Growth Equations

When a constant range of cyclic stress, $\Delta\sigma$ $(=\sigma_{max}-\sigma_{min})$, is applied to a cracked structure, stable fatigue crack growth can occur at stress levels well below the yield stress of the material. In fact, the range of the stress intensity factor ΔK, where $\Delta K = K_{max} - K_{min}$ in a cycle may also be well below the materials fracture toughness K_{Ic}. The reason for this is simple: the material near the crack tip is under severe plastic deformation (see Chapter 3). Since the stress-strain field near a crack tip is uniquely determined by the stress intensity factor, fatigue crack growth rates can be correlated to ΔK and Fig.5.1 shows a typical plot which can be divided into three zones: threshold, stable crack growth and instability.

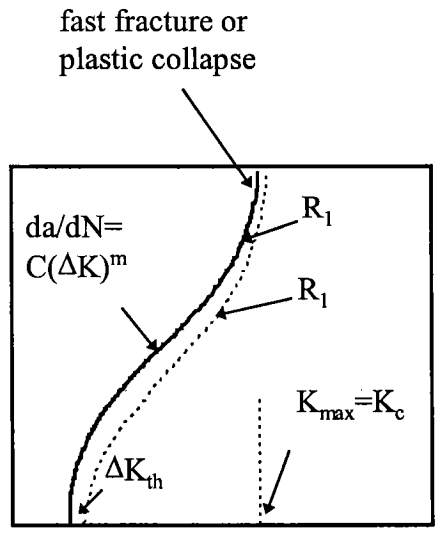

Fig.5.1 A typical fatigue crack growth Curve

In general the crack propagation rate of a given crack subjected to a constant amplitude loading depends primarily on the range of stresses in the fatigue cycle $(\sigma_{max}, \sigma_{min})$, and on the crack length. It is also influenced by the stress ratio

$R = \sigma_{min} / \sigma_{max}$. In simple cases where the condition of similitude holds, the stress intensity factor concept allows account to be taken of the two major terms by means of the stress intensity factor range,

$$\Delta K = K_{max} - K_{min} \tag{5. 1}$$

The concept of similitude is important for fatigue crack growth, as it provides the basis for applying fracture mechanics to fatigue crack growth. Similitude implies that the crack tip conditions are uniquely defined by a single loading parameter such as the stress intensity factor.

Now let us consider a growing crack under the action of a constant amplitude cyclic stress intensity. A cyclic plastic zone forms at the tip of the crack, and the growing crack leaves behind a plastic wake. If the plastic zone is sufficiently small that it is entirely embedded within an elastic singularity zone (see Examples 2.7 and 3.1), the conditions at the crack tip are uniquely defined by the current K, and the crack growth rate is characterised by K_{min} and K_{max}. If the crack is long and/or the stress is high, then crack instability and rapid acceleration can occur since K_{max} is close to the fracture toughness of the material K_{Ic}. At lower value of ΔK the linear portion of the curve in Fig.5.1 may be expressed as

$$\frac{da}{dN} = f(\Delta K, R) = C(\Delta K)^m \tag{5. 2}$$

where C and m are material, environment, stress state (stress ratio R) and temperature dependent. This equation is sometimes referred to as the Paris law. Equation (5.2), especially in its integral form, is widely used to evaluate the lifetime of cracked structures from a knowledge of the material. Usually the value of m for many engineering materials is between 2 and 4. Finally at very low ΔK values, a threshold is reached, ΔK_{th}, below which long cracks do not grow.

Experimental fatigue crack growth data are usually obtained from tests on simple specimens and are normally presented in terms of fatigue crack propagation rates (da/dN), ΔK and variations in values of R. In cases where σ_{min} is compressive the crack may close during the fatigue cycle and no clear convention for calculating ΔK has been established. Nevertheless, two popular approaches are:

1. the full range of the stress cycle will have been used, when calculating ΔK
2. only the tensile part of the cycle will have been considered, that is $\Delta K = K_{max}$.

To describe the crack growth rate over the complete range of variation, including threshold and fracture instability, a number of empirical relationships have been proposed. One example is the Pridle equation,

$$\frac{da}{dN} = f(\Delta K, R, K_c, K_{th}) = C\left(\frac{\Delta K - \Delta K_{th}}{K_c - K_{max}}\right)^m \tag{5. 3}$$

The mechanisms responsible for the threshold phenomenon are rather complicated. The most popular explanation is crack closure: due to the compressive stress induced by the plastic wake, the 'true' stress intensity factor at the tip of the crack is 'shielded' so that no plastic deformation can occur, hence no crack growth. Another possible explanation is that the crack tip plastic deformation cannot penetrate the microstructural barriers, such as grain boundaries, etc.

When a structural component is subjected to fatigue loading, a dominant crack reaches a critical size under the peak load during the last cycle leading to a catastrophic failure. As an example, consider a plate with a crack of $2a_0$ subjected to a uniform stress σ perpendicular to the plane of the crack. The total number of cycles for the crack to reach $2a_f$ can be obtained by integrating the fatigue crack propagation law given by equation (5.2),

$$N_f = \int_{a_0}^{a_f} \frac{da}{C(\Delta K)^m} \tag{5.4}$$

Using equation (2.31) we obtain

$$N_f = \int_{a_0}^{a_f} \frac{da}{C\left[Y(a)\Delta\sigma\sqrt{\pi a}\right]^m} \tag{5.5}$$

Assuming that the function $Y(a)$ is equal to its initial value $Y(a_0)$ so that

$$\Delta K = \Delta K_0 \sqrt{\frac{a}{a_0}} \quad \text{where } \Delta K_0 = Y(a_0)\Delta\sigma\sqrt{\pi a_0} \tag{5.6}$$

thereafter

$$N_f = \begin{cases} \dfrac{2a_0}{(m-2)C(\Delta K_0)^m}\left[1-\left(\dfrac{a_0}{a_f}\right)^{m/2-1}\right] & \text{for } m \neq 2 \\ \dfrac{a_0}{C(\Delta K_0)^2}\ln\dfrac{a_f}{a_0} & \text{for } m = 2 \end{cases} \tag{5.7}$$

The critical crack length a_f at which unstable crack growth occurs can be determined from fracture toughness (see Chapter 4). Usually, however, the geometry factor $Y(a)$ varies with the crack length a and the integration of equation (5.5) cannot be performed directly, but only through the use of numerical methods.

Example 5.14 A large centre-cracked plate containing an initial crack of length $2a_0$=10 mm is subjected to a constant amplitude cyclic tensile stress ranging between a minimum value of 100 MPa and a maximum of 200 MPa. Assuming the fatigue crack growth rate is governed by the equation

$$\frac{da}{dN} = 0.42 \times 10^{-11} (\Delta K)^3 \quad \text{(m / cycle)}$$

(1) Calculate the crack growth rate when the crack length has the following values $2a$=10 mm, 30 mm, 50 mm.

(2) Assuming further that the relevant fracture toughness is 60 MPa$\sqrt{m}$, estimate the number of cycles to failure.

Solution

(1) Determine the critical crack size, a_c,

$$a_c = \frac{1}{\pi}\left(\frac{K_{IC}}{\sigma_{\max}}\right)^2 = 28.7 \times 10^{-3} \quad \text{(m)}$$

This means the total crack length at fast fracture is 57.3 mm.

(2) Crack growth rates:

$$2a = 10 \text{ mm} \quad \Delta K = \Delta\sigma\sqrt{\pi a} = 12.53 \text{ MPa}\sqrt{\text{m}}$$

$$\frac{da}{dN} = 0.42 \times 10^{-11} \times (12.53)^3 = 8.26 \times 10^{-9} \quad \text{(m / cycle)}$$

$$2a = 30 \text{ mm} \quad \Delta K = \Delta\sigma\sqrt{\pi a} = 21.7 \text{ MPa}\sqrt{\text{m}}$$

$$\frac{da}{dN} = 0.42 \times 10^{-11} \times (21.7)^3 = 4.29 \times 10^{-8} \quad \text{(m / cycle)}$$

$$2a = 50 \text{ mm} \quad \Delta K = \Delta\sigma\sqrt{\pi a} = 28 \text{ MPa}\sqrt{\text{m}}$$

$$\frac{da}{dN} = 0.42 \times 10^{-11} \times (21.7)^3 = 9.24 \times 10^{-8} \quad \text{(m / cycle)}$$

(3) Fatigue life:

$$N_f = \int dN = \int_5^{28.7} \frac{da}{0.42 \times 10^{-11} (\Delta K)^3} = \int_5^{28.7} \frac{da}{7.39 \times 10^{-10} a^{3/2}} = 1.35 \times 10^9 \int_5^{28.7} a^{-3/2} da$$

$$= 1..35 \times 10^9 (-2) a^{-1/2} \Big|_5^{28.7} = 6.76 \times 10^8 \quad \text{(cycles)}$$

5.2 Effect of Stress Ratio and Crack Closure

Let us now consider the crack tip plastic deformation in more detail, as it is the driving force for crack growth. For a crack under cyclic loading, the plastic size is related to the stress intensity factor at the maximum load,

$$r_\rho = \frac{1}{\pi}\frac{K_{\max}^2}{\left(\alpha\sigma_{ys}\right)^2} \tag{5.8}$$

where α is defined in Chapter 3 and σ_{ys} refers the material's uniaxial yield stress. When the applied load is reversed, the local stress at the tip of the crack is also reversed, inducing reversed yielding. At the minimum load, the size of the reversed plastic zone is, according to superposition principle,

$$r_{pc} = \frac{1}{\pi}\frac{(\Delta K)^2}{(2\alpha\sigma_{ys})^2} \tag{5.9}$$

It is clear that for a asymmetrical loading ($R \neq -1$), $\Delta K \neq 2K_{\max}$, the maximum (sometimes called monotonic or forward) plastic zone is not equal to the reversed plastic zone, which is normally smaller than the forward plastic zone. The main reason for this smaller plastic zone is due to the residual stress induced by the maximum load. A graphical representation is shown in Fig. 5.2.

When the crack growth rates observed under different applied stress ratio R are compared, it is noted that fatigue crack growth rate exhibits a dependence on the R ratio, particularly at both extremes of the crack growth curve. While the R ratio effect on the upper end of the curve can be explained in terms of the interaction between fatigue and ultimate failure at or near K_C, the explanation for the effect near threshold is slightly more complicated.

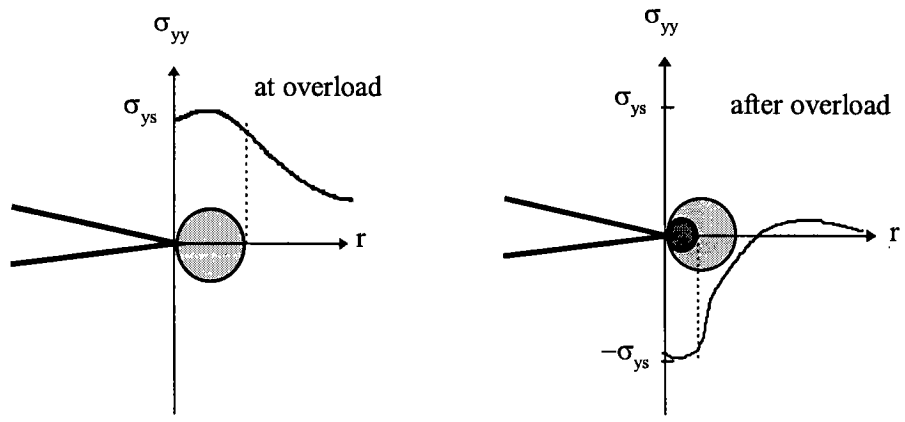

Fig.5.2 Reverse yielding at crack tip under cyclic loading

It was first reported by Elber (1971) that the elastic compliance of several fatigue specimens showed a bi-linear relationship, as depicted in Fig. 5.3. At high loads, the compliance of the fatigue specimen agreed with standard formulas for cracked specimens derived from fracture mechanics assuming monotonic loading. But at low loads, the compliance was close to that of an uncracked specimen. It was believed that this change in compliance was due to the contact between crack surfaces (crack

closure) at loads that were greater than zero. This surprising finding that fatigue cracks close at above zero load led to the postulation that the crack closure decreased the effectiveness of the applied stress intensity factor range. Crack faces (near crack tip) are in contact below K_{op}, hence the stress intensity factor range over which the crack is open is equal to $K_{max} - K_{op}$, which is defined as the 'effective stress intensity factor range', denoted as ΔK_{eff}. The main factor contributing to crack closure is the plasticity wake induced behind the crack tip. As the crack grows, plastically deformed materials remains in the region through which the crack has propagated. When the component is unloaded, the large mass of elastically loaded material compresses the small plastic region and causes regions of the crack surface to come into contact with one another before zero nominal stress is reached.

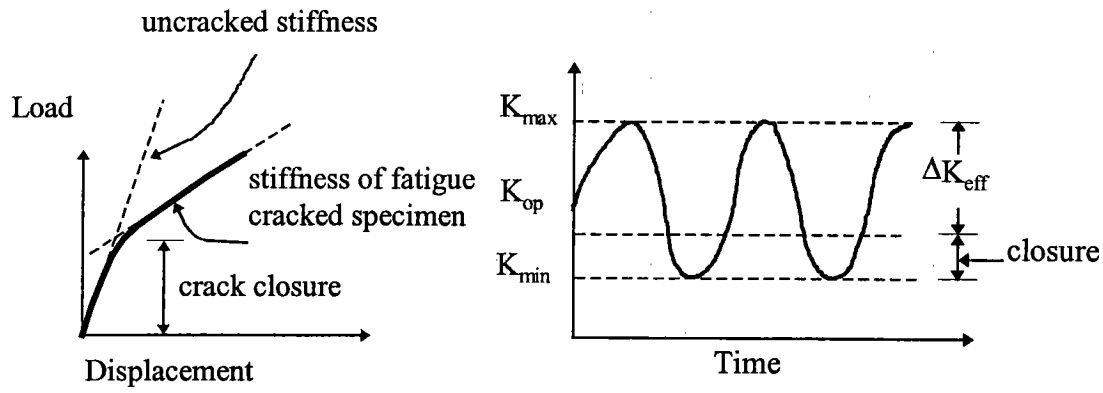

(a) Load-displacement behaviour *(b) definition of effective stress intensity factor*

Fig.5.3 Crack closure during fatigue crack growth

This concept of crack closure may be used to explain the effect of mean stress on crack propagation rates and leads to the definition of an *effective stress intensity factor range* ΔK_{eff}. At higher values of R, less crack closure tends to occur and ΔK_{eff} approaches ΔK because K_{op} approaches K_{min}. Now the fatigue crack growth equations (5.2) should be modified accordingly by replacing ΔK with ΔK_{eff}.

$$\frac{da}{dN} = f(\Delta K_{eff}) \tag{5. 10}$$

The ratio between the effective and applied stress intensity factors is normally denoted as U,

$$U = \frac{\Delta K_{eff}}{\Delta K} \tag{5. 11}$$

For instance, the effective stress ratio U for 2023-T3 aluminium at various stress ratios was reported to be independent of load levels and can be expressed as

$$U = 0.5 + 0.4R \qquad (-0.1 \le R \le 0.7) \tag{5. 12}$$

Although some researchers have argued and experimentally demonstrated that U also depends on K_{max}, it seems that there is a great deal of confusion and controversy about the K_{max} dependence of U. Nevertheless, the concept of crack closure has been widely acknowledged and demonstrated to be useful in interpreting fatigue crack growth under variable amplitude loading.

5.3 Variable Amplitude Loading

As discussed earlier, fatigue life prediction for constant amplitude loading is reasonably straightforward, provided the fatigue crack growth constants are known. However, the majority of engineering structures are subjected to fluctuating loading, and the life prediction is generally much more complicated than that outlined in the previous section. The factors that affect crack growth include variable amplitude spectrum, crack retardation due to overload, and acceleration due to underload. A number of theories and engineering methods have been proposed to reflect these effects.

Strictly speaking, for a fracture mechanics approach to be valid for fatigue crack growth under spectrum loading, the similitude condition has to be satisfied. For a crack growing in a rising or falling K field, similitude may be approximately satisfied if dK/da is small. In the case of overload, due to change in crack tip plastic deformation, similitude does not strictly hold. Simple fatigue crack growth laws that assume similitude are usually conservative when applied to variable amplitude loading. For example, a loading history can be cycle counted to identify reversals, using the rainflow or range pair method, then a linear summation of the fatigue lives of the various constant amplitude loads in the loading history would provide a first order approximation. However, such a method generally leads to conservative predictions (shorter lifetime), as it ignores the crack retardation effect to be described below.

It was first recognised empirically in the early 1960s that the application of a tensile overload in a constant amplitude cyclic load leads to temporary slower crack growth rate following the overload. Such a phenomenon is called crack retardation. In other words, the crack growth rate becomes smaller than it would have been under constant amplitude loading of the same magnitude. It was also recognised that a tensile-compressive overload following a constant amplitude cyclic load has little crack retardation effect. In fact, a compressive overload alone would accelerate crack growth. The effect of crack retardation can be better appreciated if we consider the elastic-plastic deformation ahead of a growing crack. Upon the application of a tensile overload, a large plastic zone is induced at the crack tip. After the removal of the overload, the elastic material surrounding the plastic zone acts like a clamp on this zone causing compressive residual stresses. As the crack propagates into the plastic zone, the residual compressive stresses tend to close the crack, leading to a decreasing growth rate as the crack advances into the compressive residual stress field. The effect of retardation will gradually diminish as the crack grows out of this residual stress field. It is easy to envisage that the opposite will occur for an compressive overload: the residual stress will be tensile, leading to faster crack growth.

The development in fatigue crack growth prediction can be roughly divided into three stages chronologically.

1. The first generation of crack growth analysis was based on linear assumption of constant amplitude data for da/dN versus ΔK, viz the Palmgren-Miner linear rule, which results directly from the integration of crack growth law (see next section). As the effect of loading sequence is totally ignored in this approach, the accuracy of the resulting prediction is generally poor.

2. From experimental results, a number of interactions between different load cycles of different magnitude have been observed, most notably retardation after overload and crack growth acceleration after underload. Based on these experimental findings, several plastic yield zone models, so called second generation, were proposed. The most widely used is the Wheeler model, which needs to be experimentally calibrated for a given spectrum. The main disadvantage of this type of the model is the sensitivity to loading spectrum thus rendering it impossible to be used for 'blind' predictions.

3. The third generation crack growth models, commonly called strip yield model, emerged after the discovery of crack closure by Elber (1971). When plotted against the effective stress intensity factor, which is the difference between the maximum stress intensity factor and the stress intensity factor below which crack remains closed, the effects of loading sequence and stress ratio would virtually disappear. Based on this simple fact, several models have been developed to calculate the effective stress intensity factor. For example Newman (1992; 1995). The crack opening stress level is analytically calculated using the Dugdale-Barenblatt strip yield model. After the crack has advanced a distance, a plastic wake is left behind, which in general exerts a resistance to crack closing during the downward half cycle, thus reducing the effective stress intensity which dictates crack growth rate. This plastic wake can also be (partially) destroyed if a high underload is applied, resulting in a temporary acceleration of crack growth. The essence of this method is to analytically determine the stress level required to counter act the resistance exerted by the residual plastic deformation (or the stress level above which the crack remains open), and the crack growth rate is given by the effective stress intensity factor,

$$da / dN = C\Delta K_{eff}^{m} = C(K_{\max} - K_{op})^{m} = C[(1 - S_o / S_{\max}) / (1 - R)]^{m} \Delta K^{m}$$

where constants C and m are experimentally determined from experiments. Parameter S is the applied stress, and R is the stress ratio ($S_{\min} / S_{\max}$). Clearly the only unknown in the above equation is the crack opening stress level S_o. This approach has been successfully used to correlate and predict large-crack growth rate behaviour under a wide variety of loading conditions. This is possible because the crack tip plastic deformation process that drives the crack is uniquely determined by the stress intensity factor. However, when the crack is small, the plastic strain distribution ahead the crack tip is no longer solely controlled by the stress intensity induced by the crack, but also depends on the macro-stress/strain state, which is geometry and loading dependent.

The first two methods are relatively easy to apply, while the strip yield models were more numerically involved, although this type of analysis was reported to give better

correlations to fatigue crack growth under spectrum loading. In the following, some detailed discussion of these methods is presented.

5.3.1 First Generation Model and Palmgren-Miner Linear Rule

It is easy to demonstrate the Palmgren-Miner linear damage summation rule is a direct result of crack growth rate being proportional to crack length (m=2 in the Paris law). Let an initial stress range $\Delta\sigma_1$ be changed to a different stress range $\Delta\sigma_2$ when the crack has grown from a_0 to a_1 after N_1 cycles. At the second stress range the crack grows to a_f to cause failure after N_2 cycles.

At the first stress range, from equation (5.7),

$$N_{f_1} = \frac{1}{C(\Delta\sigma_1)^2\pi}\ln\frac{a_f}{a_0} \tag{5.13}$$

$$N_1 = \frac{1}{C(\Delta\sigma_1)^2\pi}\ln\frac{a_1}{a_0} \tag{5.14}$$

hence

$$\frac{N_1}{N_{f_1}} = \frac{\ln(a_1/a_0)}{\ln(a_f/a_0)} \tag{5.15}$$

For the second stress range level

$$N_{f_2} = \frac{1}{C(\Delta\sigma_2)^2\pi}\ln\frac{a_f}{a_0}$$

$$N_2 = \frac{1}{C(\Delta\sigma_2)^2\pi}\ln\frac{a_1}{a_0} \tag{5.16}$$

hence

$$\frac{N_2}{N_{f_2}} = \frac{\ln(a_f/a_1)}{\ln(a_f/a_0)} \tag{5.17}$$

hence

$$\sum\frac{N_i}{N_{f_i}} \equiv \frac{N_1}{N_{f_1}} + \frac{N_2}{N_{f_2}} = \frac{\ln(a_1/a_0)+\ln(a_f/a_1)}{\ln(a_f/a_0)} = 1 \tag{5.18}$$

Similarly one can prove that the same conclusion can be obtained for a more general crack growth relationship,

$$\frac{da}{dN} = A\Delta\sigma^n a \tag{5. 19}$$

This is left as an exercise for the reader. Therefore the Palmgren-Miner linear summation rule assumes inexplicitly that (1) the crack growth rate is proportional to crack length and (2) the proportionality is solely dependent on the instantaneous stress level and independent of loading history. As will be seen later that assumption (2) is generally not true, owing to the crack closure effect, which is history dependent.

5.3.2 Wheeler Model

If there had been no overload, the crack would have progressed with a plastic zone of size equal to

$$r_{pc} = \frac{1}{\pi}\left(\frac{K_{\max}}{\alpha\sigma_{ys}}\right)^2 \tag{5. 20}$$

where $\alpha = 1$ for plane stress and $\alpha = \sqrt{3}$ for finite thickness, and K_{max} is the amplitude of applied stress intensity factor. At the moment of the overload the plastic zone size is

$$r_{po} = \frac{1}{\pi}\left(\frac{K_o}{\alpha\sigma_{ys}}\right)^2 \tag{5. 21}$$

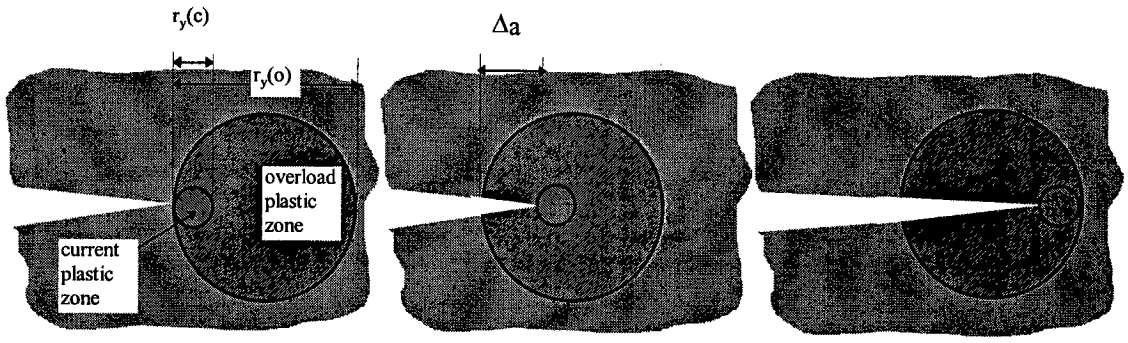

Fig.5.4 The Wheeler model for crack retardation

Wheeler assumed that retardation effect persists as long as r_{pc} is contained within r_{po}, see Fig.5.4, but the overload effects disappear when the current plastic zone touches the outer boundary of r_{po}. At any instant, the distance between the crack tip and the outer boundary of r_{po} is equal to $\Delta a + r_{pc}$, we can define two parameters

$$\lambda_1 = \frac{\Delta a + r_{pc}}{r_{po}} \quad \text{or} \quad \lambda_2 = \frac{r_{pc}}{r_{po} - \Delta a} \tag{5. 22}$$

which are plotted in Fig.5.5. A retardation factor can now be defined as

$$\phi = \lambda^{\gamma} \tag{5. 23}$$

where γ is a fitting parameter. The crack growth rate is reduced from the baseline value by ϕ:

$$\left(\frac{da}{dN}\right)_R = \phi \frac{da}{dN} \tag{5. 24}$$

An important point about the Wheeler model is that the exponent γ depends on material properties and loading spectrum. Therefore this parameter must be obtained empirically from an experiment with a stress spectrum that has a similar characteristics of that to be analysed. A variable amplitude loading analysis must be performed to determine the γ value that gives the best correlation of crack growth. The model can then be applied to structural predictions for components subjected to the same spectrum but of different magnitude. A re-calibration of the Wheeler model with new experiments must be carried out if the structure is subjected to a different stress spectrum. The linear summation method can be considered as a special case of Wheeler's model by setting $\gamma = 0$.

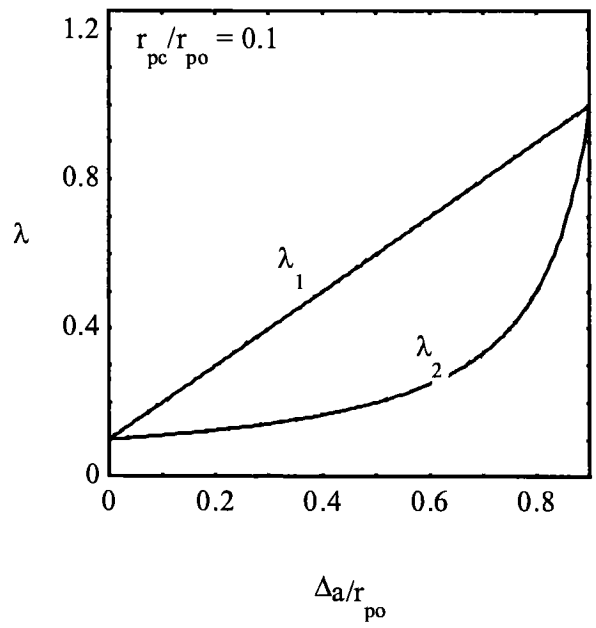

Fig.5.5 Choices of retardation parameter

5.4 Damage Tolerance Design Methodology

The term damage tolerance has a variety of meanings, but normally refers to a design methodology in which fracture mechanics analysis is used to predict crack growth life and quantify inspection intervals. This approach is usually applied to structures that are susceptible to time-dependent flaw growth. The two objectives of damage tolerance analysis are to determine (1) the effect of cracks on the (residual) strength and (2) crack growth behaviour as a function of time. Damage tolerance analysis consists of several steps. A brief outline of the steps involved in damage tolerance calculations is given below. Assuming the service loading spectrum and material properties (fracture toughness and fatigue crack growth rate constants) are known:

1. Determine the size of initial defects, e.g. NDI inspection.
2. Calculate the critical crack size at which failure would occur (see Chapter 4)
3. Integrate fatigue propagation equations to determine the number of load cycles (or blocks) for the crack to grow from its initial size to its critical size (see section 5.1)
4. Set inspection interval to half the life calculated in step 3.

A comparison between "safe-life" and "damage tolerance" design methodologies is given below.

Safe-life	Damage tolerance
structure is assumed to be defect free	initial defect is assumed to exist: equal to NDI limit
no crack formation at design service life	inspection to detect crack
design life < service life with or without repair	crack is assumed to grow to critical length in two inspection intervals
life at 1.2 design loads equal to 1.5 design life	
safe life derived from *S-N* curves (local strain approach)	crack growth determined from fracture mechanics
scatter factor of 3-4 applied to calculated lives	scatter factor = 2 in fatigue crack growth
failure probability = 0.001	failure probability after 2 inspections = 0.001

6. References

1. Anderson, T. L. (1995) *Fracture Mechanics, fundamentals and applications*, CRC Press, Boca Raton.
2. Barenblatt, G. I (1962) The mathematical theory of equilibrium cracks in brittle fracture, *Advances in Applied Mechanics*, Vol.VII, Academic Press, 55-129.
3. Battelle Columbus Laboratories (1983) *Damage Tolerant Design Handbook*, MCIC-HB-O1R, Metals and Ceramics Information Centre, USA.
4. Bowie, O. L. (1956) Analysis of an infinite plate containing radial cracks originating at the boundary of an internal circular hole, *J. Math. Phys.*, Vol. XXXV, No.1, 60-71.
5. Broek, D. (1986) *Elementary Engineering Fracture Mechanics*, Kluwer Academic Publishers, Dordrecht.
6. Broek, D. (1989) *The Practical Use of Fracture Mechanics*, Kluwer Academic Publishers, Dordrecht.
7. Dugdale, D. S. (1962) Yielding in steel sheets containing slits, *Journal of Mechanics and Physics of Solids*, Vol.**8**, 100-104.
8. Elber, W. (1971) The significance of fatigue crack closure, in *Damage Tolerance in Aircraft Structures*, American Society for Testing Materials, Philadelphia, USA, ASTM STP 486, pp.230-243.
9. Inglis, C. E. (1913) Stresses in a plate due to the presence of cracks and sharp corners, *Trans. Instn. Naval Archit.* **55**, 219.
10. Lawn, B. R. and Wilshaw, T. R. (1975) *Fracture of Brittle Solids*, Cambridge University Press, Cambridge.
11. Murakami, Y. (Editor) (1987) *Stress Intensity Factors Handbook*, Pergamon Press.
12. Muskhelishvili, N. I. (1953) *Some Basic Problems of the Mathematical Theory of Elasticity*, Groningen, P. Noordhoff Ltd.
13. Newman, J. C. Jr. (1992) FASTRAN-II - A fatigue crack growth structural analysis program, *NASA Technical Memorandum*, 104159.
14. Newman, J. C. Jr. (1995) Fatigue-life prediction methodology using a crack closure model, *J. Engineering Materials and Technology*, Vol.**117**, 433-439.
15. Rice, J. R. (1968) "A path independent integral and the approximate analysis of strain concentration by notches and cracks", *Journal of Applied Mechanics*, Vol.**35**, 379-386.
16. Timoshenko, S. P. and Goodier, J. N. (1970) *Theory of Elasticity*, Third Edition, McGraw-Hill.
17. Westgaard, H. M. (1939) Bearing pressures and cracks, *J. Appl. Mech.* Vol.**10**, 77.

18. Wheeler, O. E. (1972) Spectrum loading and crack growth, *Journal of Basic Engineering*, Vol.**94**, 181-186.

Introduction to Fracture Mechanics

C. H Wang

Distribution

AUSTRALIA

DEFENCE ORGANISATION

Defence Science and Technology Organisation

Chief defence Scientist
FAS Science Policy
AS Science Corporate Management
} shared copy

Counsellor Defence Science, London (Doc. Data Sheet only)
Counsellor Defence Science, Washington (Doc. Data Sheet only)
Senior Defence Scientific Adviser (Doc. Data Sheet only)
Scientific Adviser Policy and Command (Doc. Data Sheet only)
Navy Scientific Adviser (3 copies Doc Data Sheet only)
Scientific Adviser - Army (Doc. Data Sheet only)
Air Force Scientific Adviser

Aeronautical and Maritime Research Laboratory

Director
Library Fishermens Bend
Library Maribyrnong
Chief Airframes and Engines Division
Authors: C. H. Wang (10 copies)

L. F. R. Rose	P. Chalkley	R. Chester	A. Searl	R. Allan
M. Heller	B. Aktepe	S. Alkemade	N. Baldwin	R. Boykett
P. Chapman	G. Cole	L. Davidson	J. Donato	R. Evans
W. Foster	R. Hughes	R. Kaye	A. Kootsookos	E. Kowal
L. Krake	L.Lubacz	B. Madley	C. Martin;	G.Mcghie
L. Mirabella	L.Molent	C. Pickthall	G. Swanton	T. Tran Cong
K. Tsoi	C. Vavlitis	W. Waldman	W. Zhuang	R. Callinan

Defence Central

OIC TRS, Defence Central Library
Document Exchange Centre, DSTC (4 copies)
Defence Intelligence Organisation
Library, Defence Signals Directorate (Doc Data Sheet only)

Army

Engineering Development Establishment Library

Air Force

Aircraft Research and Development Unit
Tech Reports, CO Engineering Squadron, ARDU
OIC ATF, ATS, RAAFSIT, WAGGA
OIC ASI-LSA, DTA, HQLC

UNIVERSITIES AND COLLEGES

Australian Defence Force Academy
Library

Deakin University
Library

Flinders
Library

LaTrobe
Library

Melbourne
Engineering Library

Monash
Hargrave Library

Newcastle
Library

Syndey
Engineering Library

NSW
Physical Science Library

Queensland
Library

RMIT
Library

Tasmania
Engineering Library

Western Australian
Library

SPARES	12 copies
TOTAL	86 copies

DEFENCE SCIENCE AND TECHNOLOGY ORGANISATION
DOCUMENT CONTROL DATA

1. PRIVACY MARKING/CAVEAT (OF DOCUMENT)

2. TITLE

Introduction to Fracture Mechanics

3. SECURITY CLASSIFICATION (FOR UNCLASSIFIED REPORTS THAT ARE LIMITED RELEASE USE (L) NEXT TO DOCUMENT CLASSIFICATION)

Document	(U)
Title	(U)
Abstract	(U)

4. AUTHOR(S)

C.H. Wang

5. CORPORATE AUTHOR

Aeronautical and Maritime Research Laboratory
PO Box 4331
Melbourne Vic 3001

6a. DSTO NUMBER	6b. AR NUMBER	6c. TYPE OF REPORT	7. DOCUMENT DATE
DSTO-GD-0103	AR-009-786	General Document	July 1996

8. FILE NUMBER	9. TASK NUMBER	10. TASK SPONSOR	11. NO. OF PAGES	12. NO. OF REFERENCES
M1/9/155	DST 95/140	DSTO	73	18

13. DOWNGRADING/DELIMITING INSTRUCTIONS

Not applicable

14. RELEASE AUTHORITY

Chief, Airframes and Engines Division

15. SECONDARY RELEASE STATEMENT OF THIS DOCUMENT

Approved for public release

OVERSEAS ENQUIRIES OUTSIDE STATED LIMITATIONS SHOULD BE REFERRED THROUGH DOCUMENT EXCHANGE CENTRE, DIS NETWORK OFFICE, DEPT OF DEFENCE, CAMPBELL PARK OFFICES, CANBERRA ACT 2600

16. DELIBERATE ANNOUNCEMENT

No limitations

17. CASUAL ANNOUNCEMENT Yes

18. DEFTEST DESCRIPTORS

Fracture Mechanics; Elasticity; Fatigue; Cracking; Crack Size; Stress Analysis

19. ABSTRACT

This text is based on a series of lectures conducted on fracture mechanics. As an introductory course, the test is focused on the essential concepts and analytical methods of fracture mechanics, aiming at painting a broad picture of the theoretical background to fracture mechanics. While a brief review of some important issues in the theory of elasticity is provided in the first chapter, the main focus of the test is centred on stress analysis and energetic approaches to cracked components, local plastic deformation at crack tips, fracture criteria and fatigue life prediction.